Hierarchical diversification of instinctual behavior neurons by lineage, birth order, and sex

Najia Elkahlah[1], Yunzhi Lin[2], Troy R. Shirangi[3], and E. Josephine Clowney[2,4]

1. Cellular and Molecular Biology Program, University of Michigan Medical School, Ann Arbor, Michigan 48109
2. Department of Molecular, Cellular, and Developmental Biology, University of Michigan, Ann Arbor, Michigan 48109
3. Department of Biology, Villanova University, Villanova, PA 19085
4. Michigan Neuroscience Institute

Correspondence: jclowney@umich.edu

Abstract

Brain regions devoted to instinctual behaviors, including the vertebrate hypothalamus and arthropod cerebrum, contain bespoke neural circuits dedicated to perceptual and internal regulation of many behavioral states. These circuits are usually complex in structure and contain an extensive diversity of cell types. The regulatory mechanisms that pattern circuits for instinctual behaviors have been challenging to elucidate. Here, we developed methods in *Drosophila* to transcriptionally profile identified neuronal stem cell lineages in the cerebrum. We applied this method to lineages that generate sex-differentiated neurons with known circuit roles. We identified 91 transcription factors that, in combinations of 6–8, delineate cerebral hemilineages – classes of postmitotic neurons born from the same stem cell and sharing Notch status. Hemilineages comprise the major anatomic classes in the cerebrum and these transcription factors are required to generate their gross features. We further identified 33 transcription factors characteristic of neuronal birth order within lineages; these subtly differentiate neuronal subtypes to provide common computational modules to circuits regulating different behaviors. Our findings suggest that hemilineage and birth order transcription factors operate in a hierarchical system to build, diversify, and sexually differentiate lineally-related neurons that compose complex instinctual circuits.

Introduction

Higher processing centers in chordate and arthropod brains combine general-purpose learning regions with myriad bespoke circuits that regulate innate behaviors. These two kinds of circuits have distinct logical relationships with neurogenic cell fate diversification programs: In learning circuits, as well as spatially ordered sensory structures like the visual system, a small set of neuron types are specified in very large numbers and wire to generate repetitive columnar or layered structures. In contrast, the neurons and circuits regulating innate behaviors are each built to purpose for a unique information-processing function. Studies of neuronal cell fate diversification have historically focused on repetitive circuits, as these provided the most feasible way to explore general specification principles. The extraordinary diversity of cell types contributing to circuits for motivated behaviors – controlling drives like mating, feeding, aggression, care of offspring, and sleep – has been too difficult to address.

Yet, it is in innate behavior circuits – by definition – where developmental cell fate specification and wiring most directly dictate behavioral function. The genome somehow contains the information to build instinctual meanings of sensory stimuli and relationships among drives into the structure of these neural circuits. To explicate anatomic and functional principles underpinning these circuits and states, there is urgent need to describe the logical principles and molecular mechanisms through which their constituent neurons are patterned during development.

Three axes of diversification produce cell type diversity in the nervous system; they are used distinctly across brain regions within organisms and in different kinds of neurogenesis programs across clades (Holguera and Desplan 2018; Sen 2023). Here, we will determine how these axes pattern instinctual behavior neurons that populate the cerebrum of adult *Drosophila melanogaster*. First, neural stem cells located in specific positions in space are differentiated from one another (Lichtneckert and Reichert 2008; Urbach and Technau 2008; Briscoe et al. 2000; Jessell 2000; Sagner and Briscoe 2019). In *Drosophila*, most of the cerebrum derives from ~100 bilaterally symmetric progenitors known as Type I neuroblasts, each giving rise to distinct populations of daughter cells due to this spatial axis (Urbach, Schnabel, and Technau 2003; Urbach and Technau 2004). Second, as a neural stem cell divides asymmetrically, it progresses through expression of different transcription factors (TFs) and RNA binding proteins, and thus produces varied daughter cells over time (Z. Liu et al. 2015; Doe 2017; West et al. 2022; Clark et al. 2019; Lyu et al. 2021a; Roome et al. 2025; Konstantinides et al. 2022; Miyares and Lee 2019; Lyu et al. 2021b). In *Drosophila*, cerebral Type I neuroblasts divide ~70-100 times spanning neurogenesis windows in the embryo and larva (James W. Truman and Bate 1988). Third, sister neurons born in the same time window can assume distinct fates due to a Notch binary fate switch (Spana and Doe 1996; James W. Truman et al. 2010; Lin et al. 2012; Fiddes et al. 2018; Bello-Rojas and Bagnall 2022; Mark et al. 2021). In Type I lineages, each neuroblast division produces a ganglion mother cell, and these divide once to produce two neurons, who assume Notch-on versus Notch-off fates (Spana and Doe 1996; James W. Truman et al. 2010; Lin et al. 2012; 2010). Sex differentiation provides a fourth axis of neuronal diversification in a subset of cell types.

In Type I lineages of the arthropod central brain and ventral nerve cord, the set of neurons from the same neuroblast that shared the same Notch status form a "hemilineage" (James W. Truman et al. 2010; Lin et al. 2012; Y.-J. Lee et al. 2020). The ~100 Type I neuroblasts of the cerebrum therefore generate ~200 hemilineages; some hemilineages entirely apoptose, and the FlyWire connectome identified 183 morphological hemilineages in the adult central brain (H.-H. Yu et al.

2013; M. Ito et al. 2013; Schlegel et al. 2024; Dorkenwald et al. 2024). There is little active migration in the arthropod brain after neurogenesis, so many neural clones remain close to the sites of their birth. Neurons of the same hemilineage share the same neurite outgrowth tracts and, often, neurotransmitter system, but the two hemilineages from the same stem cell do not appear to share morphological or physiological features (Lacin et al. 2019; Larsen et al. 2009; Spindler and Hartenstein 2010; Lovick et al. 2013; Wong et al. 2013). The somata of paired hemilineages usually neighbor each other, rather than mixing, as neurite outgrowth exerts forces on the somata that pull them apart from one another. Within each hemilineage, sisters born at distinct times appear as anatomic "flavors on a theme" (H.-H. Yu et al. 2010; Lin et al. 2012; Y.-J. Lee et al. 2020). The transcriptional programs producing these major building blocks of the central brain are unknown.

To forge a path into the tremendous lineage diversity of the cerebrum, we rely on some of its best-studied cells and circuits: sex-differentiated populations used for mating (Yamamoto and Koganezawa 2013; Lenschow and Lima 2020; Oren-Suissa and Shirangi 2025; Yapici, Zimmer, and Domingos 2014). Populations of neurons become differentiated through the expression of TFs acting as the terminal effectors of somatic sex differentiation programs (Roggenbuck et al. 2024; Goodwin and Hobert 2021). In Diptera, Doublesex dominates this process in somatic tissues, and Fruitless in the central brain. At least 60 classes of cerebral neurons (~2% of neurons overall) transcribe *fruitless*, and these classes arise as subtypes of distinct hemilineages (Ryner et al. 1996, 199; H. Ito et al. 1996; Demir and Dickson 2005; Stockinger et al. 2005; Manoli et al. 2005; J. Y. Yu et al. 2010; Cachero et al. 2010; H.-H. Yu et al. 2013). *fruitless* transcripts are subject to sex-specific splicing to generate male-specific Fruitless (FruM) TFs (Ryner et al. 1996; Demir and Dickson 2005; Goodwin and Hobert 2021; Roggenbuck et al. 2024). Male-typical *fruitless* splicing is necessary and sufficient to allow male-typical mating behaviors, while the absence of FruM protein is required for female-typical behaviors such as egg laying (Demir and Dickson 2005; Hall 1978; F. Wang et al. 2020; Gill 1963). The sex-specific circuit functions of many *fruitless*-transcribing neuronal types are known, and constitute a sparse and particularly well-explored subcircuit within the larger cerebrum (K. Kimura et al. 2008; Ruta et al. 2010; Kohl et al. 2013; Clowney et al. 2015; F. Wang et al. 2020; K. Wang et al. 2021; Hoopfer et al. 2015; Manoli and Baker 2004; Lillvis et al. 2024; Koganezawa, Kimura, and Yamamoto 2016).

To ask how the transcriptional identities of *fruitless* neurons arise from, and relate to, other neurons of their hemilineages, we used a lineage tracing technique to label and isolate neurons derived from reproducibly labeled neuroblasts (Awasaki et al. 2014). Synthesizing transcriptomic, histologic, and genetic approaches, we developed methods to identify and group neurons of the same hemilineage in transcriptomic space. This allowed us to assign diverse transcription factors to their logical roles in postmitotic neurons, i.e. hemilineage patterning, birth order patterning, sex differentiation, and maturation. Overall, we found a group of 91 TFs, highly enriched for homeodomain TFs, that were expressed in combinations of 6 or more across different hemilineages. The TF combinations that exist in the central brain are very sparse compared to those possible, illustrating Waddington's idea of discontinuous cell types (Waddington 1957). In contrast, 33 TFs, likely reflecting diversification of neurons by birth order, were each expressed in subsets of neurons of each hemilineage and were from the BTB and pipsqueak families, which often have repressor functions (Brovkina et al. 2021; Mance et al. 2024; Park et al. 2024; Bonchuk et al. 2011; Janssens et al. 2022a). Most TFs in each set endured within postmitotic neurons into adulthood and thus barcode neuronal identity.

Using mAL neurons from the Notch-off hemilineage of the CREa1 neuroblast, we probed the requirement for hemilineage and birth order factors in generating gross morphological and functional properties, subtype flavors, and sex-sensitivity. mAL neurons are a *fruitless*-expressing, GABAergic population that inhibits male courtship initiation in response to gustatory pheromones of males and heterospecific females (K.-I. Kimura et al. 2005; Koganezawa et al. 2010; Clowney et al. 2015; Kallman, Kim, and Scott 2015; Hiroki Ito et al. 2016; Zhang et al. 2018). We identified a set of seven TFs from diverse protein families that mark the hemilineage in general; this TF code likely results from a transcriptional operation that combines neuroblast transcriptional status plus Notch status at neuronal birth. Each factor that we mutated disrupted CREa1B morphology. We found that distinct subsets of *fruitless* and non-*fruitless* cells in this hemilineage express distinct birth order TFs, and we could shift subtype fates by manipulating these TFs.

These findings lead us to a model of the relationship between specification of cerebral neuron types and their wiring into instinctual behavior circuits: The gross and unique features of hemilineages are determined by their combination of postmitotic hemilineage TFs, while a transcriptionally orthogonal set of birth-order-specific TFs pattern variation on the hemilineage anatomic theme. The potential for sex differentiation, via transcription of *fruitless*, derives from these two axes acting in concert and makes the most modest contribution to overall transcriptional state. These axes are arranged hierarchically, with birth order nested inside hemilineage, and sex differentiation acting on specific temporal cohorts within the hemilineage.

Results

Transcriptional analysis of developing cerebral lineages

To characterize the patterning of instinctual behavior neurons, we sought to durably label model lineages that produce neurons in the well-studied mating circuit (Figure 1A). We used an intersectional lineage tracing approach in which expression of a GAL4 within specific neuroblasts initiates a recombination cascade, resulting in permanent expression of the LexA transcription factor within its progeny (Figure 1B) (Awasaki et al. 2014). We drove lineage tracing using the R19C05 enhancer, a fragment of the *Pdfr* locus, which has been empirically shown to be expressed in the CREa1 and SMPad1 neuroblasts, among additional lineages (Figure 1B, D) (Q. Ren et al. 2016). CREa1 generates the *fruitless* mAL type; and SMPad1, the aSP-2 type (J. Y. Yu et al. 2010; Cachero et al. 2010; H.-H. Yu et al. 2013). We found that ~10 lineages were labeled reproducibly, while additional neuroblast clones were labeled sporadically. This method labels all neurons born after the completion of the recombination cascade, thus embryonically-born sisters may not be included.

We FAC-sorted labeled neurons and performed scRNA-seq on early (12hr After Puparium Formation) and mid-pupal (48hrAPF) stages to transcriptionally characterize cerebral lineages during important events in neuronal specification and circuit wiring (Figure 1D). Lineage-specific programmed apoptosis is common in the nervous system, and is often sexually differentiated, including in both mAL and aSP-2 neurons (K.-I. Kimura et al. 2005; von Philipsborn et al. 2014). In a subset of libraries, we therefore genetically blocked the completion, but not the transcriptional induction, of apoptosis by expressing the caspase inhibitor P35 (lexAop-p35) using our lineage labeling strategy (Figure 1C) (Hay, Wolff, and Rubin 1994; Q. Ren et al. 2016). Inclusion of neurons fated to apoptose, which were easily identified by their enduring high-level transcription of pro-apoptotic genes *grim*, *reaper* and *sickle*, provides access to cryptic cell types and fates. At 48h APF, we collected two libraries with the apoptotic block and two without; at 12h APF, we

collected two libraries, both with apoptosis blocked (Figure 1D). We removed optic lobe neurons, Kenyon cells, glia, and progenitors from our dataset to allow more nuanced comparisons of cerebral, Type I lineages (see Methods, and Figure S1C). We sequenced male and female neurons together and categorized them post-hoc using expression of the male-specific lncRNAs *rox1* and *rox2* (Figure S1G-H).

Within this dataset, we include five axes of neuronal diversity: Neuroblast origin, Notch diversification, birth order, sex, and maturation. Clustering using default workflows (highly variable genes across clusters) in Seurat (Hao et al. 2024a) was dominated by processes the cells were experiencing (e.g. apoptotic programs, neurotransmitter expression), rather than by the lineage relationships we sought to understand. We reasoned that measuring variable transcription factor expression would be the best way to describe neuronal diversification events (Flames et al. 2007; Hobert 2016; Sweeney et al. 2018; Yao et al. 2023). Therefore, we used transcripts of the 628 annotated *Drosophila* transcription factors, including *fruitless*, to perform semi-supervised clustering of the full dataset. After integrating time points, we tested a variety of methods and resolutions to probe how these axes of diversity related to patterns of transcription factor expression in the dataset. Surprisingly, we found that neurons did not separate by sex except at the highest resolutions; this suggests that our semi-supervised analysis method had identified durable transcription factor fingerprints associated with lineage, Notch status, and birth order. We selected an intermediate resolution based on standard bioinformatic tools, producing 52 clusters. These include some subdivisions of the 20 reproducibly labeled hemilineages, as well as clusters with lower stoichiometry likely to represent sporadically labeled lineages (see Methods and Figure 1E, S1F).

We next identified cell types that we knew were present in our dataset using expression of known markers (Figure 1G): The Notch-ON CREa1 hemilineage (CREa1A) comprises *DAT*-expressing dopaminergic neurons, while the Notch-OFF hemilineage (CREa1B) contains the *fruitless*-expressing, GABAergic mAL neurons (Y.-J. Lee et al. 2020). Cluster 14 was GABAergic, contained a subset of *fru*-expressing neurons, and included female cells that had activated the pro-apoptotic transcriptional program; we thus hypothesized that this cluster represented the CREa1B hemilineage, and that the subset of *fruitless* neurons within it were mAL neurons, most of which typically apoptose in females (K.-I. Kimura et al. 2005). We found that *DAT* expression was confined to cluster 1, which must therefore contain the CREa1A hemilineage. Cluster 1 also contained a set of apoptosing cells that derived only from the libraries containing p35 and that expressed GABAergic enzymes; we manually split this cluster into CREa1A versus the apoptosing hemilineage (Figure S1I and see Methods). We also manually split a cluster containing two well-studied antennal lobe lineages that were merged in our UMAP (Figure S1J and see Methods). We next tracked the progeny of SMPad1: The Notch-OFF SMPad1 hemilineage (SMPad1B) undergoes apoptosis, while the Notch-ON hemilineage (SMPad1A) is glutamatergic and contains *fruitless*-expressing aSP-2 neurons, which we find apoptose in females. Cluster 22 matched the expected characteristics of SMPad1A. While we didn't use neurotransmitter transcripts in clustering, we found that most clusters in our dataset expressed unified neurotransmitter systems, consistent with correspondence to hemilineages (Lacin et al. 2019). We therefore adopted the working hypothesis that hemilineage [lineage x Notch status] produces the primary variation in transcription factor expression across developing central brain neurons. Intriguingly, this is consistent with the idea that hemilineages provide the major anatomic building blocks of the arthropod brain and ventral nerve cord (Harris et al. 2015).

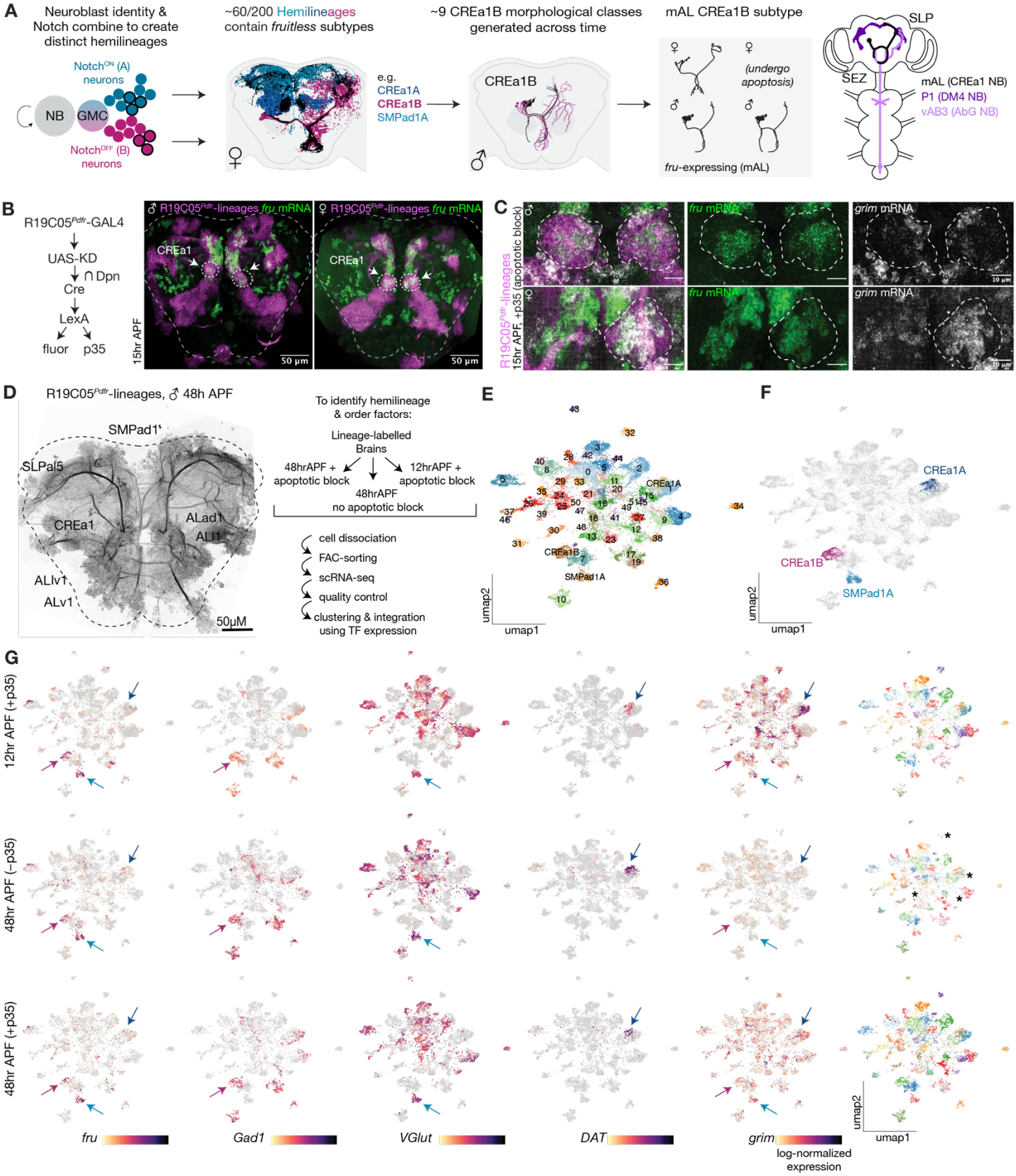

Figure 1: Transcriptional analysis of developing cerebral lineages

A. Model of hemilineage patterning in *Drosophila* Type I neuroblasts. Schematics highlighting model hemilineages are adapted from FlyWire (Zheng et al. 2018; Dorkenwald et al. 2024; Schlegel et al. 2024). The CREa1B hemilineage produces mAL neurons and other morphologies across time. Right: mAL neurons receive gustatory pheromone input,

including from vAB3, and inhibit P1 neurons to inhibit courtship (Clowney et al. 2015). Each set of neurons in the circuit transcribes *fru* and derives from a different neuroblast (NB) lineage. AbG: abdominal ganglion; SEZ: subesophageal zone; SLP: superior lateral protocerebrum. B. Intersection of 19C05 enhancer with *deadpan* allows lineage tracing of neurons born from CREa1 and other neuroblasts (immunostaining, magenta), which contain neurons transcribing *fru* (HCR RNA FISH, green). Here and throughout, dashed lines outline central brain. C. Clonal induction of p35 in the CREa1 lineage. CREa1B soma marked by immunostaining GFP induced by R19C05-lineage labelling, combined with RNA FISH for *fru* and *grim*. *grim* transcript marks neurons fated to apoptose. In the female sample shown, CREa1B is labeled in only one hemisphere, allowing comparison of the impact of p35 presence (right) or absence (left). In male, *fru* is translated into FruM and shuts off *grim*. D. R19C05-labelling, with identified hemilineages marked (some tracts are not visible) (Q. Ren et al. 2016) and sequencing workflow. E, F Cells from all libraries clustered using TF transcripts and integrated across time points. G. UMAP feature plots of scRNA-seq data from R19C05-labelled lineages, split across timepoints (12hrAPF and 48hrAPF) and conditions (+/-p35). CREa1A, B and SMPad1A marked by arrows. At right, contribution of each library type to each cluster; asterisks mark entire hemilineages that appear to naturally apoptose (i.e. observed mostly in p35 libraries). See also Figure S1.

A unique transcription factor combination defines a model hemilineage

Due to the extensive prior knowledge of the circuit function and sex differentiation of mAL neurons, we used CREa1B as a model to interrogate patterning of instinctual behavior neurons (K.-I. Kimura et al. 2005; Clowney et al. 2015; Kallman, Kim, and Scott 2015; Koganezawa et al. 2010; Koganezawa, Kimura, and Yamamoto 2016, Zhang et al., 2018). To test the hypothesis that our transcriptional clusters represent anatomic hemilineages, we first identified TFs enriched in CREa1B: *Fer1* (bHLH family, homologue of vertebrate PTF1A)*, TfAP-2* (AP-2 family, AP-2 homologue)*, fd59A* (forkhead, FoxD3 homologue)*, dsf* (nuclear receptor, NR2E1/TLX homologue)*, tup* (LIM homeobox, ISL1 homologue) and *ara* and *caup* (both TALE homeobox, homologous to IRX4) (Figure 2A,B S2D). Strikingly, these seven TFs were expressed consistently across developmental time, and none of them labeled the CREa1A hemilineage (Figure 2A, B). CREa1A was marked by *Scro*, *dmrt99B*, *erm*, *D, Lim1*, *hth, SoxN, Fer2 and CG9932* (Figure 2J, S2I). The zinc finger TFs *salm* and *salr* were also enriched in CREa1B, but only labeled a subset of cells (Figure S2E); these likely reflect more complex regulation along both hemilineage and birth order axes. The presence of *dsf* in CREa1B and *Fer2* in CREa1A are consistent with prior studies (Bou Dib et al. 2014; Duckhorn et al. 2022). Notably, *dsf* mutant males court promiscuously, consistent with a requirement for Dsf in mAL neuron function (Finley et al. 1997).

We used a set of knock-in alleles in *TfAP-2*, *dsf*, and *fd59*a, and generated a T2A-GAL4 knockin translational reporter of Fer1, to examine which neurons express each of these factors over space and time (Figure 2E, S2A-C, S2G). Across the brain, each marked a different set of other major tracts and clumps of neuronal somata, consistent with expression in diverse hemilineages and with previous studies that have identified "packets" of cerebral neurons sharing the same transcription factor (Pereanu and Hartenstein 2006). We used these morphologies, combined with RNA FISH, to validate that this transcriptional cluster corresponds to the morphological CREa1B cluster within the brain (Figure 2C-H, Figure S2A-C). All four TFs were expressed universally in the postembryonic CREa1B clone. Moreover, all four were expressed from 12h APF to adulthood, consistent with recent descriptions of hemilineage-specific transcription factors in the VNC (Figure 2I, S2D) (Soffers et al. 2025). Cross-checking expression patterns in an adult dataset of *fruitless* neurons, mAL neurons from CREa1B and PAM DANs from CREa1A continued to robustly express all the transcription factors which define them at 12 and 48h APF (MV Brovkina and EJ Clowney, manuscript in preparation). Pairs among these TFs typically labeled additional hemilineages (Figure 2I). Hemilineages sharing three factors with CREa1B were rare, and we never identified a hemilineage that shared 4 or more with CREa1B. These results support that the combination of our labeling strategy and our bioinformatic approach drives cells into their

hemilineages and allows us to test the hypothesis that combinations of TFs expressed in postmitotic neurons produce hemilineage characteristics.

Are these hemilineage TFs inherited from the CREa1 neuroblast? We used lineage tracing to ask whether any *deadpan*-positive neuroblasts had ever expressed these TFs (Awasaki et al. 2014). We found that *TfAP-2* induced labeling of other neuroblast clones, but not CREa1 (Figure S2F). *Fer1* did not induce labeling of neuroblast clones, suggesting it is not expressed in *Dpn*+ progenitors. Lineage tracing neuroblasts positive for *dsf* produced pervasive neuronal labeling (Figure S2F), resembling the pattern we saw when lineage tracing all neuroblasts, using tubulin-GAL4 (Figure S2F). Therefore, *dsf* is likely expressed in most or all neuroblasts at an early developmental time point, but isn't selective for CREa1. On the other hand, CREa1 and many other neuroblasts whose progeny are included in our dataset express *vnd* (Y.-J. Lee et al. 2020), yet we didn't observe any *vnd* expression in our postmitotic neurons (Figure S2H). Together, these results suggest that CREa1B is defined by expression of a suite of TFs that are induced in postmitotic cells and continue to barcode these cells into adulthood (Enriquez et al. 2015; Özel et al. 2022; Soffers et al. 2025). This code is not simply inherited from the neuroblast and GMC, as the hemilineage TF combinations expressed postmitotically are distinct from those in the neuroblast and in CREa1A neurons and must therefore be induced downstream of each unique [spatial x Notch] state.

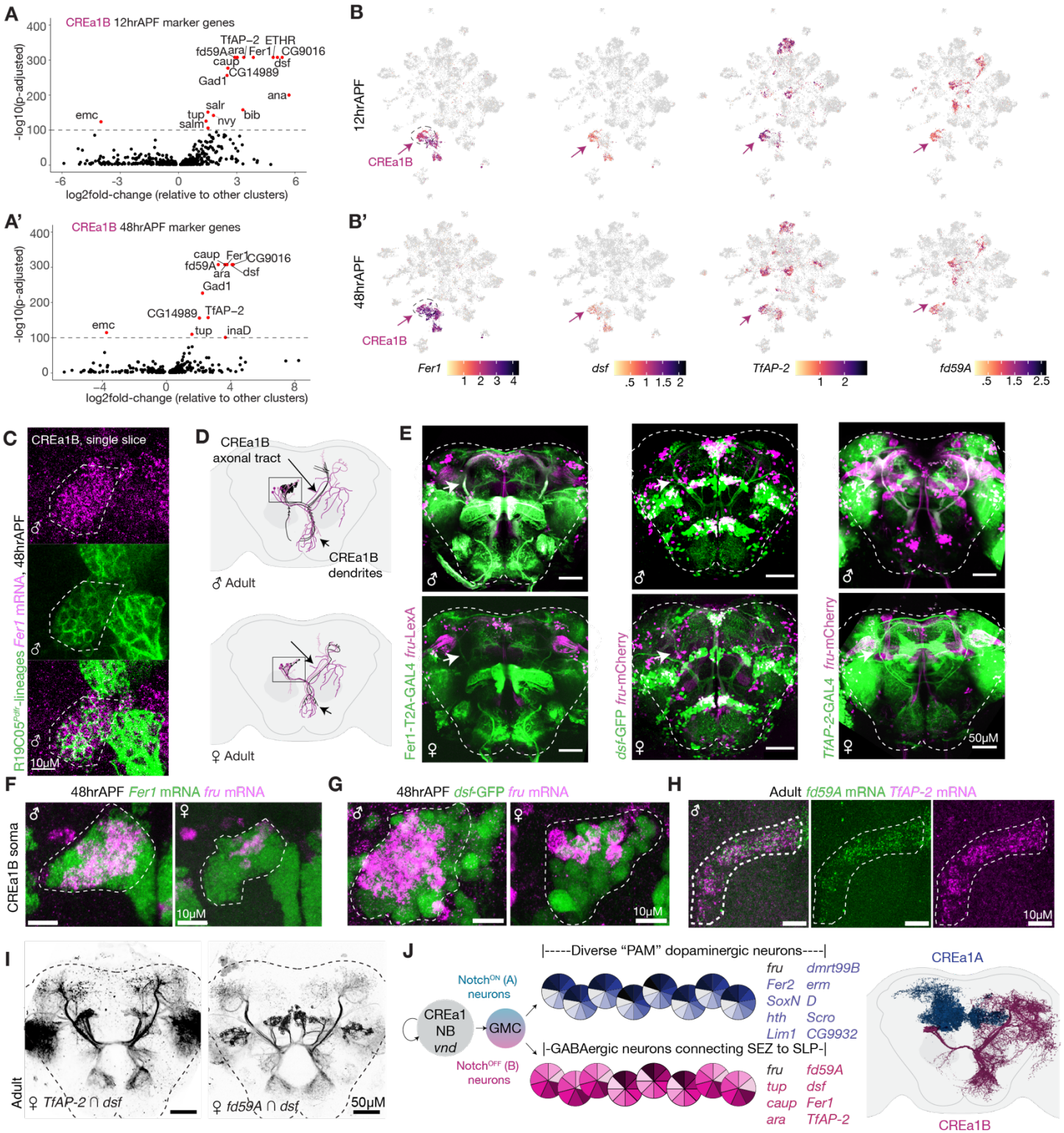

Figure 2: A unique transcription factor combination defines a model hemilineage

A. Volcano plots showing differential gene expression between putative CREa1B and other clusters in the dataset identifies hemilineage candidate factors at 12 and 48hr APF. Labelled genes: protein coding, -log10(p-adjusted) > 100 based on Wilcoxon Rank Sum test. B. UMAP plots of putative hemilineage-defining TFs in scRNAseq data from the integrated R19C05-labelled lineages split by time. C. *Fer1* RNA fills the CREa1B lineage clone (dashed outline). D. CREa1B neuronal morphologies in male and female brains; black are *fru*-expressing cells. Morphologies informed by FlyWire female connectome, CREa1 tsMARCM data, and Kimura 2005 (K.-I. Kimura et al. 2005; Zheng et al. 2018; Y.-J. Lee et al. 2020; Schlegel et al. 2024; Dorkenwald et al. 2024). E. Confocal or two photon images of neurons

expressing Fer1, *dsf* and *TfAP-2* in the central brain using knock-in GAL4 or fluorescent reporter alleles, combined with *fruitless* expression labelled with knock-in alleles. Full genotypes and generation of Fer1-T2A-GAL4 are described in the Methods. White arrows: CREa1B axonal tract. F-H. HCR RNA FISH for indicated transcription factors in CREa1B somata (outlined) at 48h APF (F-G) or adult (H). Middle panels include immunostaining of *dsf* knockin reporter. I. Two photon images of the split-GAL4 intersections of hemilineage transcription factors, labeling CREa1B neurons. J. Model of hemilineage patterning downstream of the CREa1 neuroblast. Here and throughout, two-photon imaging of native fluorescence and confocal imaging of fixed and stained brains produce slightly different brain dimensions.

Complex transcription factor combinations uniquely define hemilineages

Arthropod hemilineage identity links neurogenic origins to adult anatomy and connectivity: Years of neuroanatomical and neurodevelopmental studies have determined which neuroblasts generate adult neuronal hemilineages of the cerebrum, and recent connectomic datasets include hemilineage identity as metadata (H.-H. Yu et al. 2010; Lin et al. 2012; H.-H. Yu et al. 2013; M. Ito et al. 2013; Y.-J. Lee et al. 2020; Schlegel et al. 2024; Dorkenwald et al. 2024). Moreover, individual hemilineage anatomic units are evolutionarily ancient, and can frequently be matched across divergent arthropod species (Thomas et al. 1984; J. W. Truman and Ball 1998). Adding transcriptional fingerprints to these anatomic descriptions would allow hemilineage categorization to serve as a Rosetta Stone for solving the developmental events that build instinctual neurons and circuits of the cerebrum, especially if these fingerprints are durable across the neuron's lifetime. We therefore sought definitive TF combinations for the rest of the hemilineages in our dataset, which represents ~10% of central brain, Type I hemilineages at full stoichiometry and ~25% if we include sporadically labeled clones.

To do this, we first identified marker genes for our clusters from our integrated dataset using Seurat and then filtered the list for only transcription factors. Of 628 annotated TFs in the *Drosophila* genome, 103 were markers of subsets of our clusters (Supplemental Table 1); the majority had cluster-defining expression patterns, similar to what we demonstrated for the CREa1B-enriched TFs (e.g. see *fkh*, *Fer2* and *otp* in Figure 3). Of 102 homeodomain TFs annotated in the genome by FlyBase, 51 were included among the 103 cluster-defining TFs (Bürglin and Affolter 2016). This three-fold enrichment corresponds to the well-documented role of homeodomain TFs in neuronal diversification (Reilly et al. 2020; Briscoe et al. 2000; Xu et al. 2023). As we describe above for CREa1B, the rest of the genes are from diverse TF families. Many of the TFs in this list also overlapped with hemilineage-defining TFs in the VNC (Lacin, Zhu, et al. 2014; Allen et al. 2020; Soffers et al. 2025). Using these TF predictions along with expression patterns from the literature and/or additional histological follow-up, we were able to confirm several other matches between transcriptional clusters and anatomic hemilineages (Figure 3A, C-G).

In parallel, we blinded ourselves to TF identities and then manually inspected expression patterns of all 628 TFs across our cluster map split by developmental stage. We called 124 TFs as selective for subsets of hemilineages, of which 54 had a homeodomain fold. 33 of these 124 TFs had complex expression, i.e. they marked only precise neuronal subsets (e.g. *Clk, foxo*); marked cell classes we had mostly filtered out of our dataset (*dac* in Kenyon cells, *gcm1* and *gcm2* in glia); or reflected aspects of both lineage and birth order (e.g. *Dbx*, *RunxA*, *svp*, *luna*). We therefore retained 91 simple hemilineage TFs, of which 49 have a homeodomain fold (Figure 3A). Of the rest of the TFs in the genome, >200 were expressed ubiquitously, >150 were negligibly expressed, ~50 were associated with maturation stage, ~30 appeared associated with birth order (as we describe below) and the remainder had expression patterns that seemed a product of more than one differentiation/diversification axis (e.g. *NK7.1*). Our manual descriptions of the behavior of each

TF in the fly genome is provided in Supplemental Table 2 and select scRNAseq expression patterns are shown in Figure S3D.

We next examined how these TF sets behaved using metrics of cell-type-specificity versus maturation-specificity, as in (Jain et al. 2022); our hemilineage TFs were cell-type-specific but varied little across the maturation axis (Figure 3B). We inspected expression of each TF across our dataset of adult *fruitless* neurons (Brovkina and Clowney, manuscript in preparation). These adult *fru* neurons derive from >60 hemilineages and we have used a similar transcription-factor-based clustering to analyze them. We found that the TFs that behaved "hemilineage-ly" in our 12h APF and 48h APF neuroblast clones also marked sparse clusters in overlapping combinations in these adult cells, and we could easily match *fru* cell type across datasets using our TF combination fingerprints, as for mAL neurons, above. Using the TF codes we define here, we were also able to pick out specific hemilineages across disparate published datasets, even when those datasets were underpowered to separate neuronal subtypes (Figure 3SA-B) (Davie et al. 2018) .

While making anatomic-transcriptional matches for all the hemilineages in our dataset is beyond the scope of this manuscript, the procedure we used here can be generally deployed by other researchers with specific interests and knowledge. We hypothesize that the combinations of hemilineage-specific TFs expressed in postmitotic neurons are required to give neurons within hemilineages their shared characteristics and makes them different from other hemilineages.

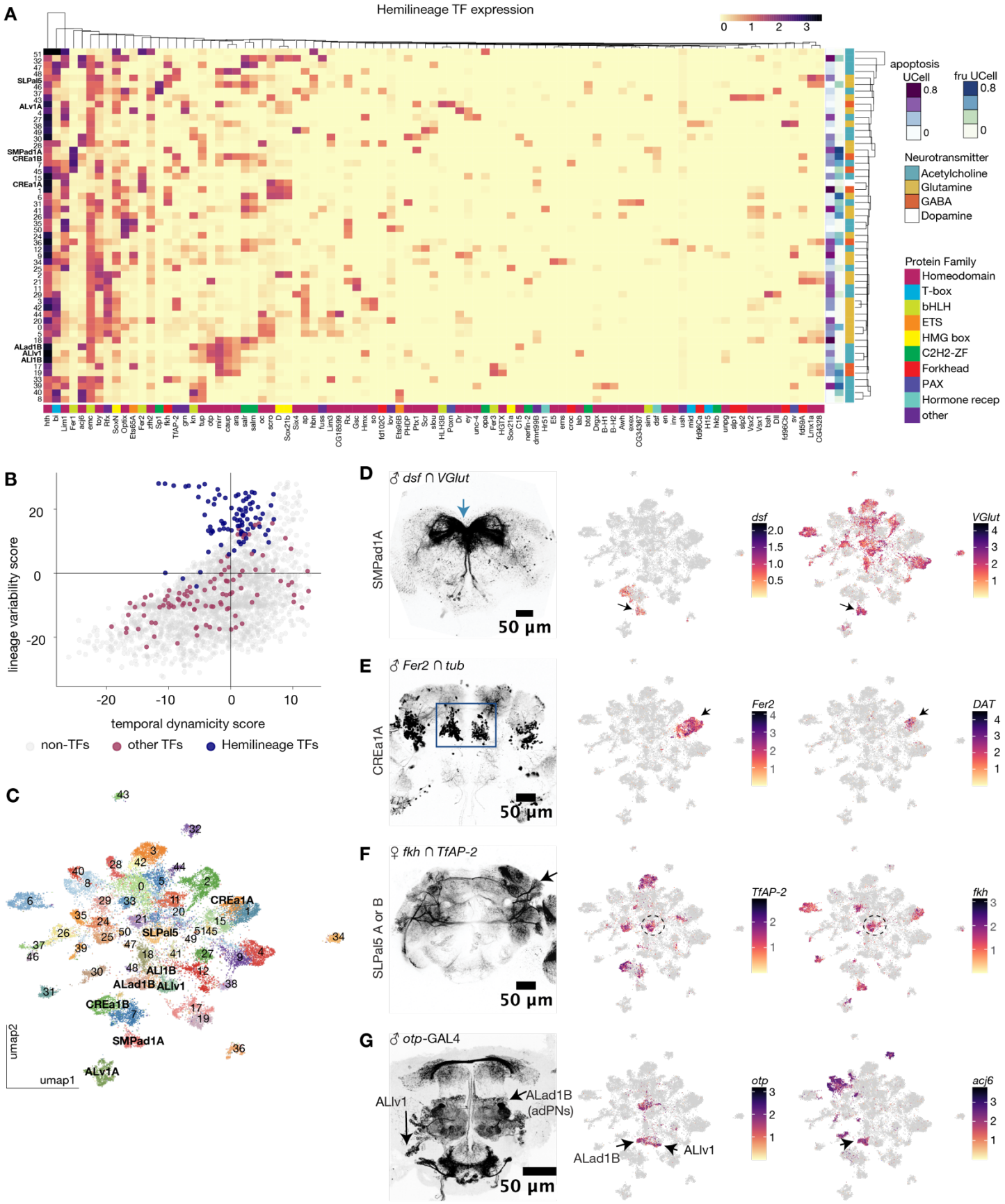

Figure 3: Complex transcription factor combinations uniquely define hemilineages

A. Heatmap displaying expression of 91 manually curated hemilineage TFs across integrated clusters. Transcription

factors were partitioned into protein families using the DAVID Bioinformatics Functional Annotation Tool and labels are displayed below (Huang, Sherman, and Lempicki 2009; Sherman et al. 2022). UCell gene set enrichment scores for neurotransmitter-related genes (*DAT*, *VGlut*, *VAChT* and *Gad1*), apoptotic programs, and *fru* are displayed at right. B. The 91 hemilineage TFs have high expression variation across clusters but low variation across developmental time. Dynamicity metric from (Jain et al. 2022). C. Clusters in the integrated dataset that we matched to morphological hemilineages. D-G: Left: Two-photon images of knockin reporters of hemilineage TFs alone or in combination with each other or other markers using split-GAL4 intersection, which allow matches of transcriptional clusters to morphological hemilineages. Right: UMAP plots displaying the log-normalized expression of the genes used to label and identify the hemilineages at left.

Identification of an orthogonal postmitotic TF code associated with neuronal birth order

In our examination of transcription factor expression patterns, we noticed a subset of TFs that were expressed in swathes of neurons within each hemilineage cluster (Figure 4B). A universal birth order code for postmitotic central brain neurons has not been previously described, to our knowledge. To identify additional factors with this expression pattern, we measured variance of each of the 628 TFs across clusters, within clusters, and along the maturation axis (Figure 4A). We identified >30 TFs with high variance within clusters and low variance across clusters, and cross-checked this with our manual annotations above. Through this approach, we identified a total of 33 factors, including *br, pdm3, dan, danr, hb, bab1, bab2, Eip93F, ab, mamo, dati,* and *chinmo*. The RNA binding protein *Imp* was expressed in a similar pattern, while *Syp* was universally expressed (Z. Liu et al. 2015) (Figure S4D). Several of these genes have been shown to act as temporal factors in neuroblasts and/or to label subsets of post-embryonically-born neurons within the same VNC or central brain lineage (Z. Liu et al. 2015; Lin et al. 2012; Zhu et al. 2006; L.-Y. Liu et al. 2019; Maurange, Cheng, and Gould 2008; Syed, Mark, and Doe 2017; Kohwi, Hiebert, and Doe 2011). This birth order series was distinct from the temporal progression of intermediate neural progenitors (INPs) in Type II lineages and had only minimal overlap with temporal TFs in postmitotic optic lobe neurons (Bayraktar and Doe 2013; Konstantinides et al. 2022; Tang et al. 2022; Simon et al. 2025). Some factors were expressed consistently across 12 and 48h APF stages, while others were enriched at one or the other (Figure S4C). Most continued to be expressed in matched types of adult neurons (Brovkina and Clowney, manuscript in preparation), and therefore cannot simply be leftovers from the neuroblast. We hypothesized that these TFs select for distinct terminal identities within a hemilineage according to the order that neurons are born.

We next wanted to verify that putative birth order factors truly label subsets of neurons across many hemilineages. Br and Pdm3 have previously been shown to allocate postmitotic neurons to alternative fates (Smolin et al. 2024; Özel et al. 2022). We focused on their expression, along with Mamo and Imp, in our R19C05-traced hemilineages. Using immunohistochemistry, Br and Pdm3 labeled subsets of neurons within hemilineages throughout the brain and had nearly mutually exclusive expression (Figure 4E). The 33 putative birth order TFs are enriched for annotated transcriptional repressors and many contain BTB (*ab, br, mamo, chinmo*) or pipsqueak (*dan, danr, Eip93F*) domains, or both (*psq*, *CG3726*, *bab1*, *bab2*) (Figure 4F-G) (Brovkina et al. 2021; Mance et al. 2024; Park et al. 2024; Bonchuk et al. 2011; Janssens et al. 2022a).

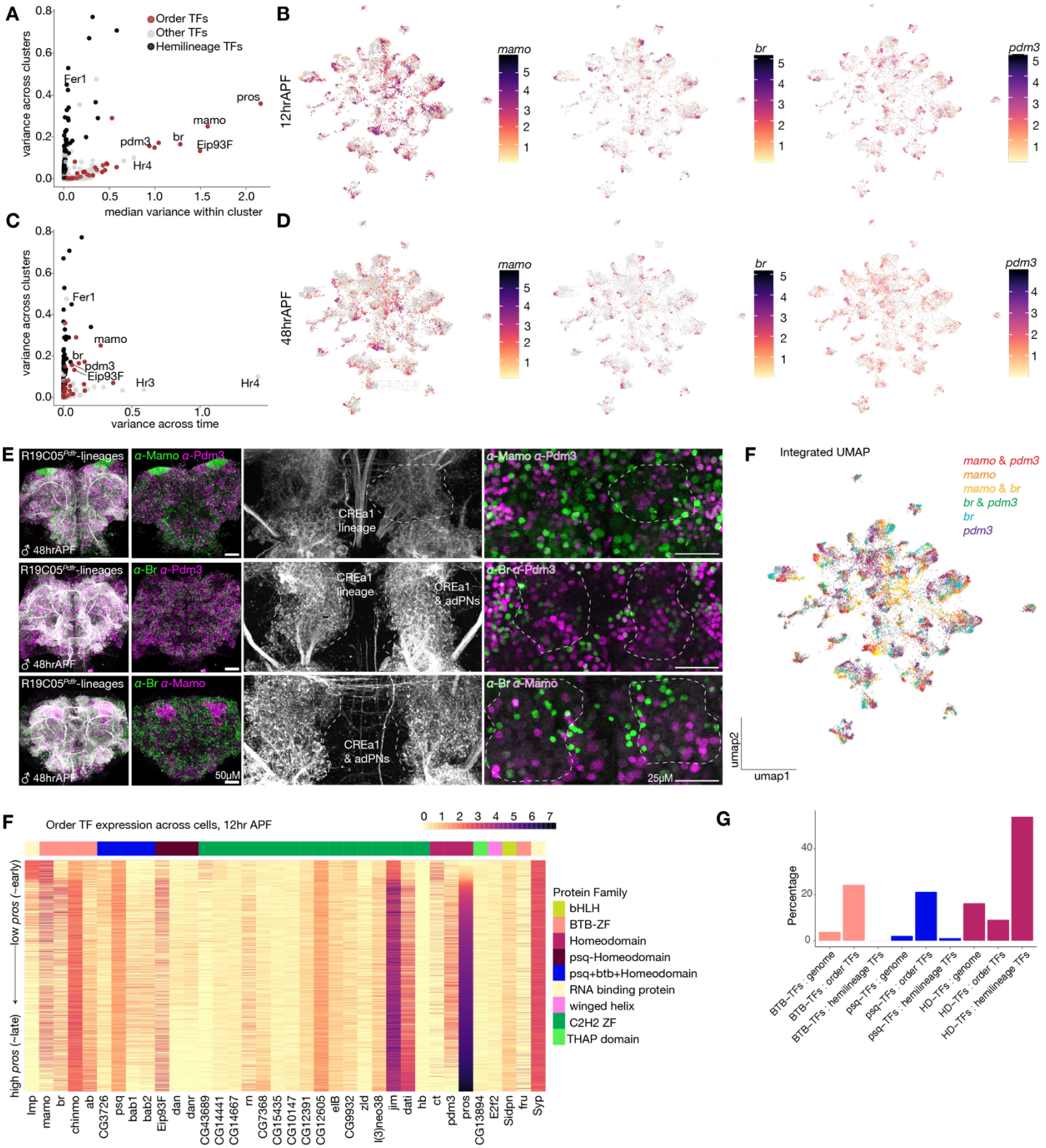

Figure 4: Identification of an orthogonal postmitotic TF code associated within neuronal birth order
A,C. Putative birth order factors have high variance within clusters but low variance across clusters (A) and across maturation time (C). B,D. Featureplots showing expression of select birth order factors within clusters, split by time. E. Confocal images of R19C05 neuroblast clones combined with immunostaining for putative birth order TFs. These proteins are largely non-overlapping within hemilineages (CRE1B, dashed outline) and their representation in subsets of neurons is nearly universal across hemilineages. F. Integrated UMAP showing the distribution of cells within hemilineage clusters that express different sets of birth order factors. F. Heat map showing cell-wise expression (rows)

of 33 birth order TFs (columns), together with *fru* and the RNA binding proteins Imp and Syp. Rows are sorted by expression of *pros*, which roughly stratifies early- to late- born cells. Columns are sorted by protein functional domains, shown at bottom. G. Representation of protein domains among TFs in the genome, or among hemilineage or birth order sets.

Hemilineage TFs are independently required for shared hemilineage features

We hypothesize that hemilineage TF combinations are important to specify hemilineage development. To address this, we focused on CREa1B. We examined null mutants of *fd59a* and *dsf*, which survive to adulthood, and used the 19C05 driver to generate CREa1B clones with *TfAP-2* knockdown. In all three cases, we see a clear disruption to CREa1B development: Removing *fd59A* or *TfAP-2* produced severed morphological defects, where the typical axonal tracts and dendrites were often completely gone (Figure 5A&E). In *dsf* mutants, CREa1B neurite tracts are intact, but dendritic and axonal anatomy are disrupted (Figure 5I). In each case morphological disruptions are shared by *fru* and non-*fru* neurons within CREa1B, suggesting these factors regulate morphology similarly across neuronal subtypes within a hemilineage.

We also asked how each factor impacted the number of cells within CREa1B and distribution of *fru* expression. Our previous work suggested that *fru* is induced by distinct regulatory mechanisms across different cell types (Brovkina et al. 2021), and here we did not find any one-to-one correspondence of hemilineage or birth order TFs with *fru* expression (Figure 3 & 4). In *dsf* mutants, we saw that the overall number of CREa1B cells decreased, while the number of *fru* cells increased (Figure 5J, Figure S5C). In *fd59a* mutants, we saw modest and sex-specific changes in the distribution of *fru* and non-*fru* cells in the hemilineage (Figure 5B, Fig S5A). In our *TfAP-2* knockdown CREa1B clones, we see a severe drop in the number of *fru* mAL neurons in both sexes, and a corresponding drop in the overall number of neurons in the hemilineage in males (Figure 5F, Figure S5B). Most mAL neurons are programmed to apoptose, but are spared in males by FruM's suppression of pro-apoptotic gene transcription (Figure 1C) (K.-I. Kimura et al. 2005). This normally results in the retention of ~30 mAL neurons in males, and only ~5 in females (K.-I. Kimura et al. 2005). The most parsimonious explanation of the *TfAP-2* knockdown data (loss of *fru* expression in both sexes, severe loss of neurons only in male) is that TfAP-2 is required in CREa1B for *fru* expression. In females, loss of *fru* transcription is observed; in males, loss of *fru* and FruM unmasks the apoptotic program, reducing the size of the hemilineage.

These results confirm that hemilineage-specific combinations of transcription factors are critical for the development of neuronal features. For TfAP-2, the effects we observe must be cell autonomous in postmitotic neurons, as we knocked the gene down clonally and we know it is not expressed in the CREa1 progenitor. We suspect that the complex Dsf phenotype may be due to both fate specification events in the CREa1 progenitor and regulation of terminal feature development in neurons, and will test this hypothesis elsewhere.

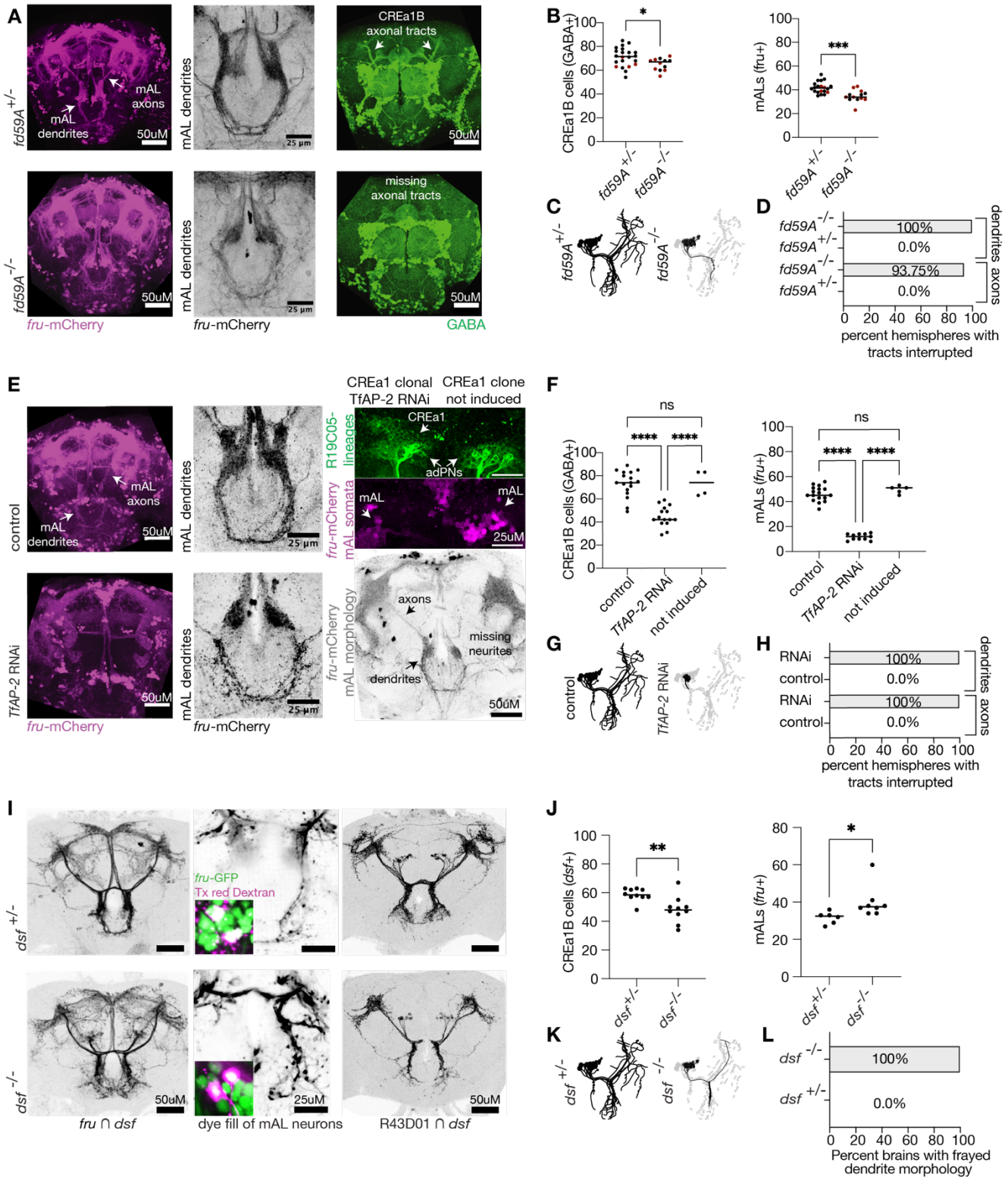

Figure 5: Hemilineage TFs are independently required for shared hemilineage features
(Samples analyzed throughout this figure are male; female samples and additional analyses can be found in Figure S5.) A. Morphology of mAL neurons labelled by *fru*-mCherry or GABA immunostaining in controls versus *fd59a* mutants. Left and right panels, whole brain views, middle panels display mAL neuron dendrites zoomed in. Arrows, mAL axons or dendrites. B. Left: Number of CREa1B neurons (GABA+). Right: mALs per hemisphere (*fruitless*-expressing). Significance: unpaired t-test; here and throughout, *: p<0.05, **: p<0.01, ***: p<0.001, ****: p<0.0001. C. schematic displaying effect of loss of *fd59A* on CREa1B morphology. D. Summary of the qualitative effect of the

loss of *fd59A* on mAL axonal and dendritic morphology. n is shown by the number of points in (B). E. Morphology of mAL neurons labelled by *fru*-mCherry in controls versus *TfAP-2* RNAi clones. Middle panel displays mAL neuron dendrites zoomed in, and the last image panels show control and *TfAP-2* RNAi clones within the same brain. The CREa1B soma are labelled by R19C05-lineage labeling and mAL neurons soma and morphology are labelled using *fru*-mCherry. Arrows, mAL axons or dendrites. F. Left: the number of total CREa1B neurons (GABA+). Right: the number of total mALs per hemisphere (*fruitless*-expressing). Significance, one-way ANOVA. "Non-induced" refers to hemispheres from animals of the *TfAP-2* RNAi genotype in which clonal labeling of CREa1 was not induced, while "control" refers to the genotype lacking the RNAi allele. G. Schematic displaying the effect of losing *TfAP-2* on CREa1B morphology. H. The qualitative effect of the loss of *TfAP-2* on mAL axonal and dendritic morphology. I. Left: Morphology of mAL neurons labelled by intersection of *dsf* and *fru* in controls versus *dsf* mutants, middle panel: Texas red Dextran electroporated into the mAL axonal tract in control and *dsf* mutants; insets showing somata indicate that dye fill is restricted to *fru*-expressing cells in the lineage. Representative of three or more experiments per genotype. Last image panel shows the intersection of R43D01 and *dsf* labelling, which includes *fruitless*-expressing and non-expressing CREa1B neurons. J. Left: the number of total CREa1B neurons (*dsf*+). Right: mALs per hemisphere (*fruitless*-expressing). Significance: unpaired t-test. K. Schematic displaying the effect of losing *dsf* on mAL morphology. L. Summary of the qualitative effect of losing *dsf* on dendritic morphology.

Birth order factors differentiate mAL neurons and sex-shared sisters

Next, we asked whether putative birth order factors can delineate CREa1B neuronal subtypes. Different hemilineages produce different numbers of neuronal subtypes, up to 40 unique types produced by the antennal lobe lineages (H.-H. Yu et al. 2010; Lin et al. 2012; Y.-J. Lee et al. 2020). 9 morphological subtypes of CREa1B neurons have been identified and ordered using tsMARCM birthdating (Y.-J. Lee et al. 2020). We subclustered CREa1B and found 7 transcriptional clusters across our integrated timepoints (Figure 6B). Given CREa1B is a sexually dimorphic hemilineage, we first broadly split CREa1B subtypes into *fru* mAL neurons and non-*fru* sisters. We combed the literature for cells with morphology resembling the non-*fru* sisters and identified the mlSEZt neurons, which are labeled by R29F12 (NetA fragment)-R55E01 (CG15803 fragment) split Gal4 (Deere et al. 2023). These neurons appear to play an analogous circuit role to mAL neurons, gating feeding in response to flavors, where mAL neurons gate mating in response to pheromone tastes (Deere et al. 2023; Clowney et al. 2015; Kallman, Kim, and Scott 2015; Snell et al. 2022; Chen and Dahanukar 2020). Clusters 5 and 6 expressed *NetA* and *CG15803* but lack *fru*, suggesting these are the mlSEZt's (Figure 6B). We then compared the anatomy of mlSEZt neurons to mAL neurons labeled using a *fru* reporter; we confirmed that these are non-overlapping populations, and saw that the morphology of the non-*fru* mlSEZt neurons of both sexes is remarkably similar to the morphology of the *fru* mAL neurons of females, which also lack FruM (Figure 6A). We note that there are several other non-*fru* CREa1B neuronal subtypes visible in EM connectomes, in tsMARCM data, and in the expression patterns of our driver lines. Based on birth ordering from tsMARCM and other heat-shock-based methods, unidentified sisters with complex dendritic "wings" are born first, then the mlSEZt's, then the *fru* mAL's, and then one other unnamed, non-*fru* sister type, which has antler-shaped axons and truncated dendrites (Y.-J. Lee et al. 2020). Antler and winged types are likely contained within CREa1B subclusters 1 and 2; our transcriptional analysis is underpowered to subdivide the winged types, which each occur only once per hemisphere.

To ask about the transcriptional diversity of mAL neurons, we looked at *fru* expression in our CREa1B cluster and found that mAL neurons are split into clusters 3 and 4 (Fig 6B). Each of these clusters contained cells from males and females, suggesting that these clusters are not yet split by events downstream of FruM. We found that mAL and mlSEZt neurons could be subdivided by distinct birth order factors: mlSEZt neurons were enriched for *rn* and *mamo*, mAL cluster 4 for *br* and *Eip93F* and mAL cluster 3 for *pdm3*, *dan* and *danr* (Figure 6C&F). By immunohistochemistry,

we found that most mAL neurons expressed either Pdm3 or Br, and not both, demonstrating that these are bone fide mAL subsets (Figure 4E, 6E). Interestingly, we found that the *Drosophila* proapoptotic genes *grim* and *skl* were enriched in the *pdm3* subset versus the *br* set, and that nearly all the *pdm3*-expressing female cells arose from the libraries in which we blocked apoptosis (Figure 6F, S6B). Thus we infer that *pdm3* mAL neurons are the ones that initiate programmed cell death, which is blocked by FruM in male, while *br* mAL neurons are those normally retained in females (K.-I. Kimura et al. 2005). As Kimura 2005 showed that the apoptosing *fru* neurons are the later-born, we conclude that *br* cells are born first, and then *pdm3* cells; though tsMARCM birth dating in females leaves open the possibility that these fates alternate (Y.-J. Lee et al. 2020).

To view these distinct mAL clusters in the brain, we used split-GAL4 drivers to intersect *pdm3* or *br* expression with hemilineage-defining *TfAP-2*. We found that the *TfAP-2*, *pdm3*-expressing mAL set was indeed absent in the female; in the male, all *TfAP-2*, *pdm3* cells had the male-typical "horsetail" shape (Figure 6G). Intersection of *br* and *TfAP-2* included both sex-differentiated and sex-shared CREa1B cells, consistent with our transcriptional data, in which *br* expression straddled the transition from non-*fru* to *fru*. We verified that non-apoptosing female mAL neurons were within the *br* set by intersecting *br*, *TfAP-2*, and *fru* (Figure 6G). Blocking cell death in CREa1B equalized the proportion of mAL types between the sexes (Figure S6C).

We compared transcription between the *pdm3* versus *br* mAL subsets (Figure 6F). Strikingly, the *pdm3* sets from males and from females in which apoptosis was blocked expressed the neuropeptide Dh31, while the *br* sets did not; thus when the *pdm3* cells apoptose in females, *Dh31* expression is completely lost (Figure 6F, H S6A). Together, these results suggest that the main role for FruM in the *pdm3* mAL subset is to block apoptosis by suppressing expression of *grim* and *skl*, and that Dh31 peptide will be male-specific in wild type mAL neurons due to regulation of apoptosis by FruM, not direct induction of *Dh31* (Figure S6A&B). On the other hand, seven genes were downregulated in male versus female *br* mAL cells (Figure 6H, right, Figure S6D). These included a neuronal adhesion molecule (*DIP-delta),* a neuropeptide *(Nplp1)* and an RNA-binding protein *(mbl).* Because we showed previously that FruM represses its direct targets, these male-suppressed genes are consistent with direct regulation by Fruitless protein to sexually differentiate this mAL subtype (Brovkina et al. 2021). Overall, we see that the difference in transcription between birth-order subtypes within a hemilineage (i.e. mlSEZt, versus mAL *pdm3*, vs mAL *br*) is greater than differences between sexes (i.e. mAL *br* male versus female, mAL *pdm3* male versus female). This suggests sexual differentiation of neurons is tweaking a sex-shared ground plan rather than producing a completely different cell type in the male.

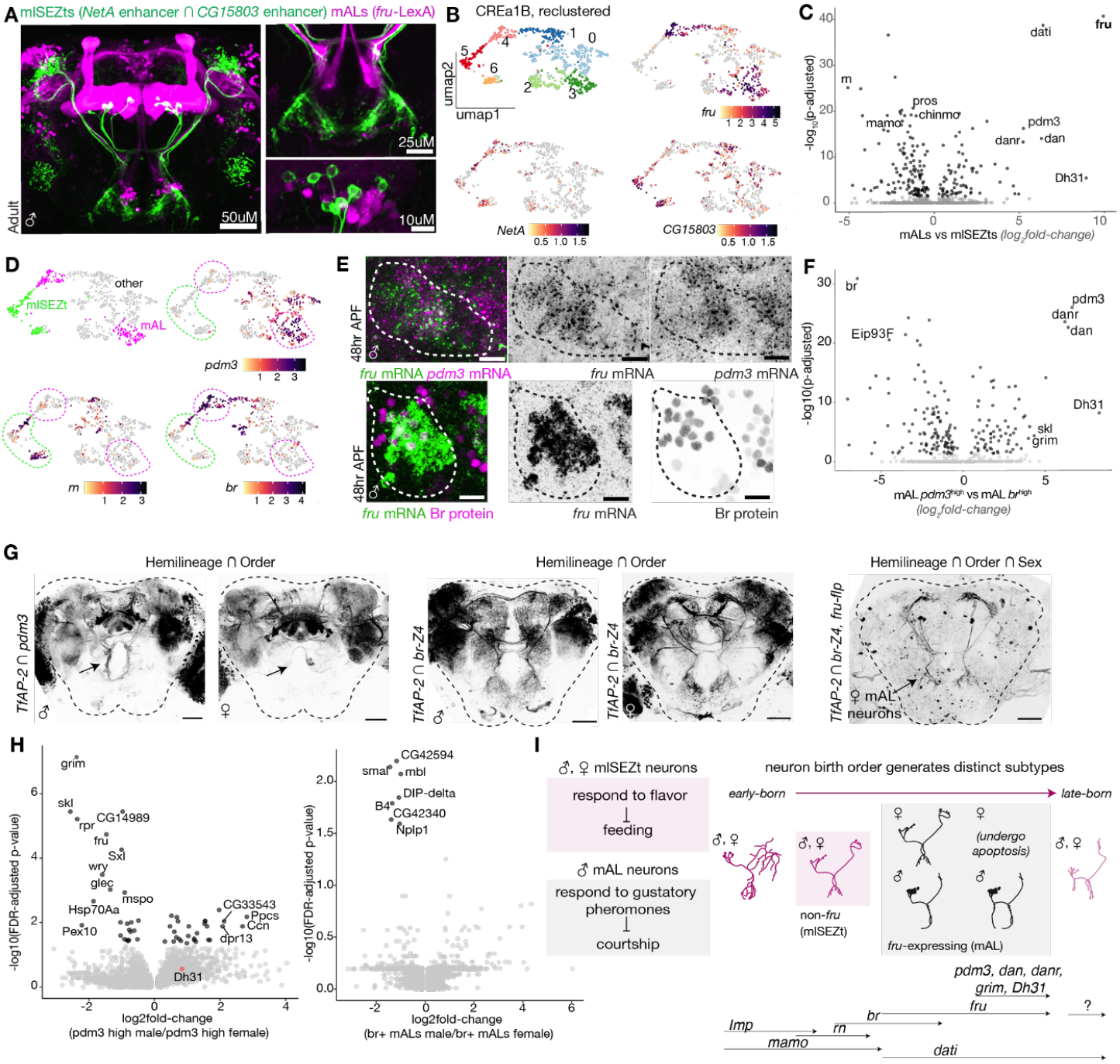

Figure 6: Birth order TFs differentiate mAL neurons and sex-shared sisters

A. Comparison of mlSEZt and mAL neurons. At left, maximum intensity projection of confocal stack, at right, substacks focused on dendrites or somata. mlSEZt somata lack *fru*. B. UMAP of subclustered CREa1B, integrated across time. Featureplots display log-normalized expression of mAL and mlSEZt markers (*NetA, CG15083, fru*). Subclustering was performed using all variable features. C. Volcano plot showing differential gene expression between mAL neurons and mlSEZts. Black dots, significant based on Wilcoxon Rank Sum test. Gene labels highlight putative birth order factors, *fru* and *Dh31*, as described in the text. D. CREA1B UMAP plots showing mAL and mlSEZt types separated by birth order TFs (*rn*, *pdm3* and *br*). E. CREa1B soma (outlined based on *dsf* reporter expression, not shown) with RNA FISH against *fru* and *pdm3* (top) and RNA FISH against *fru* and immunostaining against Br (bottom) at 48hrAPF. F. Volcano plot showing differential gene expression analysis between *pdm3* versus *br* mAL neurons. Black dots, significant based on Wilcoxon Rank Sum test. Gene labels highlight putative birth order factors, cell death genes and *Dh31*, as described in the text. G. Two-photon images of split-GAL4 intersections of hemilineage TFs *TfAP-2* with birth order TFs *br* and *pdm3*, with or without intersection with *fru*. H. Volcano plots showing differential gene expression analysis between male versus female *pdm3* or *Br* mAL neurons. Left: Black dots,

significant based on Wilcoxon Rank Sum test. Pink dot, *Dh31*. Labels: protein coding genes, with average log2FC > 2 or < -2 or -log10(FDR-adjusted p-value) > 2.5 based on Wilcoxon Rank Sum test. Right: Black dots and labelled genes, significant based on Wilcoxon Rank Sum test. I. Schematic displaying circuit roles and likely birth order of CREa1B subtypes, and expression of order TFs, *fruitless*, *Dh31* and *grim*.

Birth order TFs program hemilineage subtypes

To ask whether manipulating the birth order factors within a hemilineage can shift the fates of neurons, we overexpressed *pdm3* in CREa1B cells using *dsf*-intersect-*TfAP2* split-GAL4. We verified that this genetic strategy was restricted to postmitotic neurons by using the split-GAL4 to drive lineage labeling using the Awasaki strategy; no lineages were labeled. We found that overexpression of *pdm3* altered the total number of *fruitless* mAL neurons in the female but not the male, suggesting Pdm3 induces the cell death fate and FruM protein is sufficient to block it even in a wider window, i.e. in cells that would usually be of the *br* mAL type (Figure 7A&A'). Indeed, we saw a reduction in the total number of CREa1B neurons, suggesting Pdm3 could induce cell death outside of the *fru* window (Figure S7A). However, we did not see a complete loss of cells, indicating that Pdm3 is insufficient to induce cell death in the entire CREa1B hemilineage (Figure S7A). We also see loss of the typical "mlSEZt" ring-shaped axon, loss of "wing" dendrites, and increase in the "antler" CREa1B type upon *pdm3* overexpression (Figure 7A&A'). To ask whether the order TFs regulate the expression of each other as they can do in VNC neuroblasts and in the visual system, we examined the effect of *pdm3* overexpression on Br expression (Doe 2017; Konstantinides et al. 2022). We found that Br protein persists in CREa1B despite overexpressing *pdm3* (Figure S7B&B'), suggesting that these proteins can be co-expressed. However, this does not rule out regulatory relationships among the 33 order TFs in general. Overall, our data suggest that Pdm3 could be important for cell death within CREa1B and for the specification of late-born mAL and antler CREa1B neuronal subtypes at the expense of earlier-born wing and mlSEZt types.

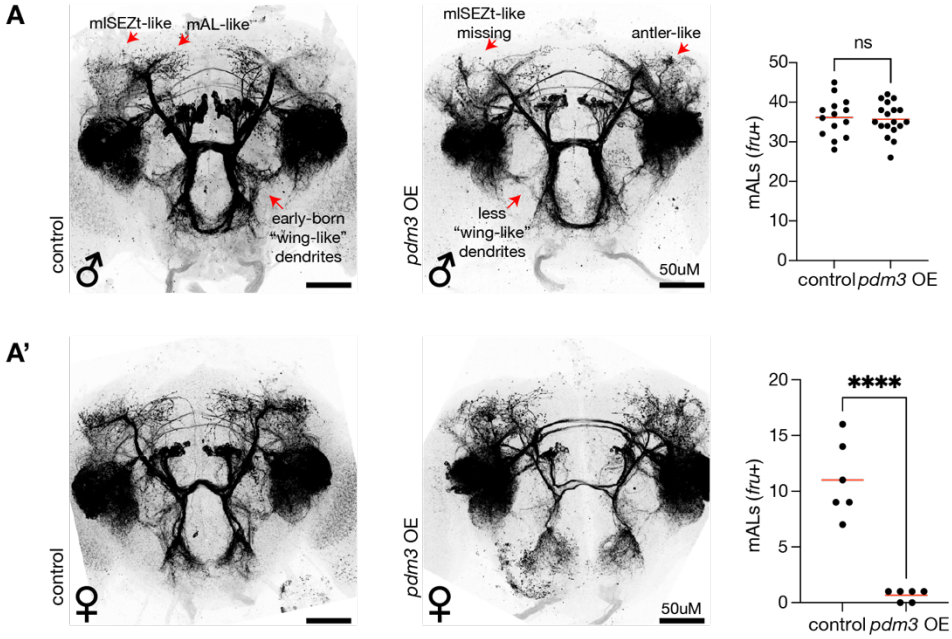

Figure 7: Birth order TFs diversify hemilineage neuronal fates

A. The Split-Gal4 intersections of *dsf* and *TfAP-2* in control (left) versus Pdm3 overexpression (right) in males (top) and females (bottom). Red arrows highlight structures of CREa1B axonal and dendritic subtypes. Right: Number of total mAL neurons (*fruitless*-expressing) per hemisphere in males (top) and females (bottom). Significance: unpaired t-test.

Discussion

Here we describe a model for the diversification of rare neuronal types with unique behavioral roles. While instinctual behaviors are well studied at the circuit and behavioral level, the transcriptional logic generating these immensely diverse cell types has been obscure. By capturing and sequencing postmitotic neurons of identified Type I lineages of the arthropod cerebrum, we identified two orthogonal TF codes, one of which diversifies hemilineages, and the other the sister neurons within hemilineages. The hemilineage transcription factor combinations that we find in postmitotic neurons are distinct from those patterning the stem cells that generate them, while the birth order code shares many members with other temporal regulatory events in neurogenesis and metamorphosis. Expression of most hemilineage and birth order transcription factors we identify is durable within specific populations of neurons from before metamorphosis through adulthood and thus serve as barcodes of identity both in a causal developmental sense and from our position as observers of the brain. Our model therefore decomposes these "terminal selectors" or "morphology transcription factors" into two groups defined by the separable developmental axes that induce them (Enriquez et al. 2015; Hobert 2016). Finally, both hemilineage and birth order factors set the table that sex differentiation acts on (Roggenbuck et al. 2024).

Transcriptional patterning and circuit wiring of lineally related neurons

The developmental axes that dominate diversification of transcription, anatomy, and physiology differ across regions of the arthropod brain and generate distinct circuit wiring patterns. Anterior brain lineages occur only once per hemisphere and thus serve singular computational roles, but the dominance of hemilineage in their patterning resembles recent findings in the ventral nerve cord (Urbach, Jussen, and Technau 2016; Allen et al. 2020; Soffers et al. 2025). In contrast, the degree of spatial diversification of neurons in the arthropod visual system is lower, while the transcriptional and morphological differences produced across birth orders is higher (Konstantinides et al. 2022; Özel et al. 2022; Simon et al. 2025).

At the circuit level, work in the VNC has shown that hemilineages can act as functional units and that temporal identity diversifies their connections (Harris et al. 2015; Mark et al. 2021). In line with this model, mlSEZt neurons and the sexually dimorphic mAL neurons within the cerebral CREa1B hemilineage are inhibitory neurons that relay taste information from the subesophageal zone to neurons in the superior lateral protocerebrum. Shared hemilineage identity – encoded by TFs including Dsf, TfAP-2, Fd59a, and Fer1 – provides CREa1B neurons with their major neurite outgrowth tract and physiological computation; their birth order identity – encoded by expression of Rn and Mamo versus Pdm3 or Br – specifies the fine shape of their axons and dendrites and thus their precise connectivity and behavioral role. The result is that male mAL neurons receive gustatory pheromone inputs and project to P1 neurons to gate mating initiation, while mlSEZt neurons of both sexes receive flavor information and connect to non-P1 downstream targets to gate feeding (Clowney et al. 2015; Kallman, Kim, and Scott 2015; Sengupta et al. 2022; Deere et al. 2023). Identifying whether the female mAL neurons are functionally distinct from the morphologically similar, sex-shared mlSEZt's would shed light on the neural circuitry underlying female behaviors and the role of lineage in circuit wiring. Where these sister neurons of cerebral hemilineages supply a common computational module to distinct circuits, the columnar organization of visual system circuits results from lineally related neurons wiring together. Across species, a variety of developmental relationships are likely exploited to produce circuits with varied connectivity logic.

Extant TF codes vs potential TF codes

We have not found factors in postmitotic neurons that could separate the spatial identity of their neuroblast of origin versus Notch status. Notch effectors were no longer visible in postmitotic neurons at the time points we analyzed, and hemilineage pairs from the same neuroblast (e.g. CREa1A, B) did not share TFs with each other. In neuroblasts, the expression patterns of dozens of TFs have been shown to correlate with spatial position (i.e. A-P, D-V, medial-lateral) (Urbach and Technau 2004). We have not yet identified TFs participating in hemilineage codes that reflect simple spatial axes. Moreover, we generally did not see the same spatial factors in neuroblasts and in postmitotic hemilineages: *vnd* is expressed in many of the neuroblasts whose progeny we analyzed, yet was not detected in postmitotic neurons (Y.-J. Lee et al. 2020). *TfAP-2* and *Fer1* were expressed in postmitotic CREa1B cells, but not in the CReA1 stem cell. While this will require further study, these results together suggest that there is a "translation event" at neurogenesis whereby the spatial factors in the neuroblast combine with the Notch switch to produce unique hemilineage TF codes (Mark et al. 2021; Sen 2023). Kenyon cell neurogenesis, which does not involve Notch diversification and thus does not produce hemilineages, may be an exception that proves the rule–KC neuroblasts and postmitotic KCs share expression of *eyeless* (Noveen, Daniel, and Hartenstein 2000; Kurusu et al. 2000). On the other hand, type I neuroblasts and differentiating daughters appear to use many of the same temporal factors; whether these are strung together in the same order and whether the temporal code in the daughter matches the temporal code in the neuroblast at the time of its birth, or is offset, remains to be seen.

We were struck by the apparent excess of TFs devoted to hemilineage patterning: The 91 postmitotic hemilineage TFs we identify, taken 7 at a time, could generate nearly a billion unique combinations, yet there are only 200 cerebral hemilineages. Thus, the TF combinations that exist in the brain are a very sparse subset of the combinations that could be formed from the individual factors; this excess diversity explains why we could recover most TFs with hemilineage-specific expression from our initial subsampling of lineages. Recent analyses in the visual system have found that the amount of transcriptional diversity that could be produced by the available transcription factor set is also far in excess of the number of cell types actually made (Simon et al. 2025). Because we observe heterogeneity in the rate at which each is expressed (e.g. from >⅓ of hemilineages for Lim1 or bi to <1/10% for *croc* and *unc-4*) and repeated relationships among certain groups of TFs (*ara, caup, mirr; CG4328, Lmx1a; Fer1, dsf*), combinations that actually exist are unlikely to be a random subsample of those possible. Finally, mutating single hemilineage factors did not cause conversion to a different cell type/hemilineage (Arlotta and Hobert 2015). Instead, we observed generally perturbed axons and dendrites, suggesting that hemilineage factors, while independently required, are sufficient to build ground plans only in specific cocktails. Hemilineages are deeply conserved in insects and can be identified in disparate clades by their characteristic neurite outgrowth tracts (Thomas et al. 1984; J. W. Truman and Ball 1998). By adjusting effector genes downstream of these handles, evolution can subtly alter the terminal characteristics of neuronal development; by altering the handles themselves, evolution could produce novel neuronal ground plans.

Development reuses TFs to generate diverse neurons

To our knowledge, the temporal transcription factor series patterning larvally born neurons of the cerebrum has not yet been identified. The 33 factors we highlight here are strong candidates based on their expression patterns and because several have already been shown to be important neuroblast factors and/or to have roles in temporal patterning, including *chinmo*, *Eip93F, mamo,*

br, *dan*, and *hb* (Syed, Mark, and Doe 2017; L.-Y. Liu et al. 2019; Kohwi and Doe 2013; Zhu et al. 2006). Some of our birth order transcription factors (*br* and *pdm3*) and our hemilineage factors (*TfAP-2, fd59A*) have been identified as terminal selectors in the optic lobe (Konstantinides et al. 2018; 2022; Özel et al. 2022; Smolin et al. 2024; Simon et al. 2025). These data indicate that, during development, the same transcription factors can occupy different roles across different parts of the nervous system to diversify neuronal types. Moreover, as we describe in Figures 3 and 4, not all transcription factors expressed in subsets of hemilineages or subsets of neurons within them can be assigned to a single diversification axis—various factors reflect more than one axis (e.g. [hemilineage x birth order], [birth order x maturation]). Factors such as Clock and Fru are induced with exquisite specificity, likely downstream of the hemilineage and birth order axes, in neuronal types that form subcircuits relevant to specific classes of behaviors. Finally, different cerebral lineages produce very different degrees of neuronal diversity, up to the ~40 anatomically distinct cell types from antennal lobe lineages (H.-H. Yu et al. 2010; Lin et al. 2012). Such stem cells have been shown to produce more ground plan variety than the "two hemilineages per neuroblast" rule, and may thus rely on additional transcriptional substructure.

Lineage-dependent induction and function of Fruitless

Through our analysis of sexually differentiated hemilineages, we did not find hemilineage or birth order TFs or combinations universally correlated with *fruitless* across cell types. We found that *fruitless* can be expressed in both A and B hemilineages, in all the cells of a hemilineage, in one birth order window, or in multiple. *Fruitless* being expressed in just a subset of neurons within a hemilineage could indicate that it is repressed in non-*fruitless*-expressing neurons, possibly due to the action of birth order factors. Overall, our data suggest that there are many ways to achieve *fruitless* expression, like neurotransmitter identity (Konstantinides et al. 2018; Serrano-Saiz et al. 2020; Kim et al. 2020), and this is in support of our previous findings that diverse enhancers within the *fruitless* locus drive expression in distinct *fruitless* cell types (Brovkina et al. 2021). It also supports the idea that *fru* expression is more akin to a terminal feature of diverse neurons than it is a patterning factor.

Transcriptional sex differences are like a mirage, mostly created by wholesale removal of certain neuron types. Our approach of restoring lost cells by blocking cell death allowed us to identify truly analogous cell types between the sexes. Using this method, we found that Fruitless sexually differentiates neurons differently even across temporal windows of the same hemilineage. The transcriptional differences between matched cell types that are actually present in both sexes are remarkably subtle. Indeed, during our analysis we found greater transcriptional differences across hemilineage cell types (birth order windows) versus for identical [hemilineage x birth order] types across sexes. In male versus female *fruitless* neurons of the same hemilineage and birth order, we found on the order of 10 genes to be differentially expressed; these were related to cell death (*grim* and *rpr*), synapse organization (*DIP-delta*), and intriguingly, RNA regulation (*mbl*).

Transcriptional mechanisms of cerebral neuron diversification

How do hemilineage and birth order TFs generate the hierarchical diversity of neurons regulating instinctual behaviors? In the cerebrum, we found that manipulation of shared hemilineage factors had dramatic effects on neuronal morphology, with a complete loss of both axons and dendrites in some cases, while manipulation of a birth order transcription factor altered the "flavor" of the neuron while preserving the overall theme of the hemilineage. Given these phenotypes, we favor the hypothesis that hemilineage TF cocktails function in concert to activate enhancers needed to

pattern gross neuronal ground plans and functional features. In contrast, we found BTB/POZ and pipsqueak transcription factors to be enriched within the order transcription factors. Methodologically diverse recent studies, including our own, have shown that Fruitless and other BTB/POZ TFs in the Tramtrack family are strong repressors (Brovkina et al. 2021; Janssens et al. 2022b; Mance et al. 2024; Park et al. 2024; Bonchuk et al. 2011). We posit that sex differentiation and birth order differentiation, while induced by distinct upstream mechanisms, use the same molecular mechanism – closing hemilineage-specific enhancers – and produce analogous developmental impacts – patterning neuronal variation on the hemilineage theme (Sen et al. 2019). In other parts of the nervous system, where sister neurons are far more different from each other, a different regulatory logic may apply. Alternatively, researchers working in the neural tube proposed the model that enhancer opening is performed in common across lineages, and that spatial diversification of neurons occurs entirely through transcriptional repression (Bailey et al. 2006; Muhr et al. 2001). To discriminate between these models will require determining the regulatory valence of hemilineage TFs and defining whether they act on the same or different enhancers as birth order TFs.

Acknowledgments
We thank Tzumin Lee, Haluk Lacin, Yu-Chieh David Chen, Neşet Özel, Ted Erclik, Mubarak Syed, and Uwe Walldorf for developing and sharing critical fly alleles, composite genotypes and antibodies, without which this work would not have been possible. We also thank the Bloomington Drosophila Stock Center. Margarita Brovkina provided conceptual and technical input. Veronica Sikora collected mlSEZt images and Joseph Carter generated Fer1-T2A-GAL4. FAC-sorting was performed with Kamlai Saiya-Cork in the BRCF Flow Cytometry Core. Funding was provided by NINDS DSPAN F99 award (F99NS139459), the CMB NIH T32 GM145470, and the CMB NIH T32 GM007315 to NE; McKnight Scholar Award, Pew Biomedical Scholar Award, and startup funds from the University of Michigan to EJC; and National Science Foundation (IOS-1845673) to TRS.

Methods
Fly husbandry: Flies were maintained on Bloomington food with a yeast sprinkle ("B" recipe, Lab Express, Ann Arbor, MI) at 25C on a 12:12 light-dark cycle with at least 60% humidity (provided by a beaker of water in the incubator). For staging developmental time points, pupae were marked at the 0hr APF "white pupae" stage. Animals for scRNAseq were collected +/−1-2 hours from the stated developmental time points (e.g. 48hr APF were collected from 47-49hr APF).

Fly genotypes by Figure

Figure	Genotype
Fig 1B-D, Fig S1B, Fig 2C:	Dpn<KOT<CREpest;Act^ds^Lp65,lexA-op2-myrGFP/lexAop-p35;20xUAS-KD1/GMR19C05-GAL4
Fig 2E: (Fer1)	lexAop-tdTomato;Fer1-T2AGAL4/ 10xUAS-IVS-myr::GFP
Fig 2E: (dsf)	Mi{y[+mDint2]=MIC}dsf[MI09213];fru[MI05459][mCherry]
Fig 2E: (TfAP-2)	lexAop-tdTomato;TfAP-2-GAL4/ 10X-UAS-IVS-myr::GFP
Fig 2F:	Canton-S
Fig 2G:	Mi{y[+mDint2]=MIC}dsf[MI09213]; tm2 or TM6B

Fig 2H:	w1118
Fig 2I (left):	dsf-GAL4DBD, 10X-UAS-IVS-myr::GFP; TfAP-2GAL4AD
Fig 2I (right):	dsf-GAL4DBD, 10X-UAS-IVS-myr::GFP; fd59A-VP16
Fig S2A (left):	Dpn<KOT<CREpest;Act^ds^Lp65,lexA-op2-myrGFP/lexAop-p35;20xUAS-KD1/GMR19C05-GAL4
Fig S2A (right):	Canton-S
Fig S2B:	lexAop-tdTomato;Fer1-T2A-GAL4/ 10xUASIVSmyrGFP
Fig S2C:	UAS>stop>GFP; fru-flp/Fer1-T2A-GAL4
Fig S2F: (left)	Dpn<KOT<CREpest;Act^ds^Lp65,lexA-op2-myrGFP;20xUAS-KD1/ TfAP-2-GAL4
Fig S2F: (middle)	Dpn<KOT<CREpest;Act^ds^Lp65,lexA-op2-myrGFP;20xUAS-KD1/ dsf-GAL4
Fig S2F: (right)	Dpn<KOT<CREpest;Act^ds^Lp65,lexA-op2-myrGFP/lexAop-p35;20xUAS-KD1/tub-GAL4
Fig 2G:	tub-GAL4-DBD;UAS-2X-eGFP/fd59A-VP16
Fig 3D:	dsf-GAL4DBD, 10X-UAS-IVS-myr::GFP/VGlut-GAL4AD; TM2 or TM6B/+
Fig 3E:	tub-AD-GAL4, UAS-2X-eGFP;IF or CyO; Fer2-DBD-GAL4/ Dr[1] or TM3, sb
Fig 3F:	UAS-GFP/ IF or CyO; TfAP-2AD;fkh-DBD
Fig 3G:	otp-GAL4/ CyO; FruMiMIC[mcherry]/10X-UAS-IVS-myr::GFPP
Fig 4E:	Dpn<KOT<CREpest;Act^ds^Lp65,lexA-op2-myrGFP/lexAop-p35;20xUAS-KD1/GMR19C05-GAL4
Fig 5A (control):	P{ry[+t7.2]=neoFRT}40A P{w[+mW.hs]=FRT(w[hs])}G13 fd59A[2] bw[1] speck[1]/+ ; fru[MI05459][mCherry]/+
Fig 5A (fd59A mutant):	P{ry[+t7.2]=neoFRT}40A P{w[+mW.hs]=FRT(w[hs])}G13 fd59A[2] bw[1] speck[1]/ P{ry[+t7.2]=neoFRT}40A P{w[+mW.hs]=FRT(w[hs])}G13 fd59A[1] bw[1] speck[1] ; fru[MI05459][mCherry]/+
Fig 5E (control):	act>stop>Gal4-2, UAS-flp;10xUasIVSmyrGFP; CyO or SP; GMR19C05-Gal4, fru[MI05459][mCherry]; tm2 or tm6b
Fig 5E (TfAP-2 mutant clones):	act>stop>Gal4-2, UAS-flp;10X-UAS-IVS-myr::GFP; UAS-TfAP-2 RNAi; GMR19C05-GAL4, fru[MI05459][mCherry]; Uas-Dicer
Fig 5I (dsf control, left):	dsf-GAL4/pJFRC79-8X-lexAop2-FlpL (attp40); fru-LexA/pJFRC41-10XUAS-FRT-STOP-FRT-myr::GFP (su(Hw)attp1)
Fig 5I (dsf mutants, left):	dsf-GAL4/*dsf*^{Del}, *pJFRC79-8XLexAop2-FlpL* (attp40); *fru*^{LexA}/*pJFRC41-10XUAS-FRT-STOP-FRT-myr::GFP* (su(Hw)attp1)
Fig 5I (middle panel, top), Fig S5D (left):	dsf-GAL4/+; Mi{y[+mDint2]=MIC}fru[MI05459][GFP]/+
Fig 5I (middle panel, bottom), FigS5D (right):	dsf-GAL4/*dsf*^{Del}; Mi{y[+mDint2]=MIC}fru[MI05459][GFP]
Fig 5I (dsf control, right):	dsf-LexA/pJFRC79-8XlexAop2-FlpL (attp40); R43D01-Gal4 (attp2)/pJFRC41-10XUAS-FRT-STOP-FRT-myr::GFP (su(Hw)attp1)

Fig 5I (dsf mutants, right):	dsf-LexA/*dsf*^{Del}, *pJFRC79-8XLexAop2-FlpL* (attp40); *R43D01-Gal4* (attp2)/*pJFRC41-10XUAS-FRT-STOP-FRT-myr::GFP* (su(Hw)attp1)
Fig 6A:	P{y[+t7.7] w[+mC]=R29F12-p65.AD}attP40/lexAop-TdTomato; P{y[+t7.7] w[+mC]=R55E01-GAL4.DBD}attP2/ *fru*-lexA,10X-UAS-IVS-myr::GFP
Fig 6E (top):	dsf-lexA/+; 13X-lexAop2-IVS-myr::GFP/+
Fig 6E (bottom):	Mi{y[+mDint2]=MIC}dsf[MI09213]; tm2 or TM6B
Fig 6G (left):	UAS-GFP/+; TfAP-2AD;pdm3-DBD
Fig 6G (middle):	Br-Z4DBD; UAS-GFP/ p or CyO; TfAP-2AD;pdm3-DBD
Fig 6G (right):	Br-Z4DBD; UAS>stop>GFP;TfAP-2-AD, fru-flp
Fig 7A & A' (left):	dsf-GAL4DBD, 10X-UAS-IVS-myr::GFP/+; TfAp-2AD/+
Fig 7A & A' (right):	dsf-GAL4DBD, 10X-UAS-IVS-myr::GFP/UAS-pdm3-long; TfAP-2AD/+
Fig S7B & B' (top):	dsf-GAL4DBD/CyO or SP; TfAP-2AD/Mi{y[+mDint2]=MIC}fru[MI05459][GFP]
Fig S7B & B' (bottom):	dsf-GAL4DBD/UAS-pdm3-long; TfAP-2AD/Mi{y[+mDint2]=MIC}fru[MI05459][GFP]

Fly alleles

Reagent	**Source**	**Citation**
Dpn<KOT<CREpest;Act^ds^Lp65,op2-myrGFP/CyO;20xUAS-KD1/TM6B	Tzumin Lee Lab	(Awasaki et al. 2014)
w[1118]; P{y[+t7.7] w[+mC]=GMR19C05-GAL4}attP2	Bloomington Drosophila Stock Center (BDSC): 48842	(Jenett et al. 2012)
w[1118];lexAop-p35	FBtp0116088	Barry Dickson, unpublished
;;Fer1-T2A-Gal4	Clowney Lab	This paper
y[1] w[*]; Mi{y[+mDint2]=MIC}dsf[MI09213]	BDSC: 52083	(Nagarkar-Jaiswal et al. 2015)
;; fru[MI05459][mCherry]	Clowney Lab	This paper
FruP1-LexA (III)	BDSC 66698	(Mellert et al. 2010)
lexAop-tdTomato.Myr (su(Hw)attp5)	FBti0160868	César Mendes, Columbia University, unpublished
10XUAS-IVS-myr::GFP {attp2}	BDSC 32197	(Pfeiffer, Truman, and Rubin 2012)
TfAP-2 GAL4	Haluk Lacin	(Lacin et al. 2020)

TfAP-2-AD	Haluk Lacin	(Lacin et al. 2020)
dsf-DBD	Troy Shirangi	(Diamandi et al. 2024)
fd59A-VP16	Gift from David Chen	unpublished
dsf-GAL4	Troy Shirangi	(Duckhorn et al. 2022)
dsf-LexA	Troy Shirangi	(Diamandi et al. 2024)
y[1] w[*]; P{w[+mC]=tubP-GAL4}LL7/TM3, Sb[1] Ser[1]	BDSC: 5138	(T. Lee and Luo 1999)
y[*] w[*] P{w[+mC]=UAS-2xEYFP}AX; wg[Sp-1]/CyO; P{w[+mC]=Tub-GAL4DBD.D}3	BDSC: 60297	(Diao et al. 2015)
y[1] w[*]; P{w[+mC]=Tub-dVP16AD.D}2, P{w[+mC]=UAS-2xEGFP}AH2; Dr[1]/TM3, Sb[+]	BDSC: 60295	(Diao et al. 2015)
w[*];Mi{Trojan-p65AD.2}VGlut1[MI04979-Tp65AD.2]/CyO	BDSC: 82986	(Lacin et al. 2019)
Fer2-DBD	Gift from David Chen	(Chen et al. 2023)
fkh-DBD	Ted Erclik	(Soffers et al. 2025)
otp-GAL4	Uwe Walldorf	(Hildebrandt et al. 2022)
w[1118]; P{ry[+t7.2]=neoFRT}40A P{w[+mW.hs]=FRT(w[hs])}G13 fd59A[1] bw[1] speck[1]/CyO, P{ry[+t7.2]=ftz-lacB}E3	BDSC 56819	(Lacin, Rusch, et al. 2014)
w[1118]; P{ry[+t7.2]=neoFRT}40A P{w[+mW.hs]=FRT(w[hs])}G13 fd59A[2] bw[1] speck[1]/CyO, P{ry[+t7.2]=ftz-lacB}E3	BDSC: 56820	(Lacin, Rusch, et al. 2014)
y[1] w[*] P{w[+mC]=GAL4-Act5C(FRT.CD2).P}D	BDSC: 4779	(Pignoni and Zipursky 1997)
P{w[+mC]=UAS-FLP.Exel}1, y[1] w[1118]	FBst0008208 BDSC: 8208	Annette Parks of Exelixis, Inc.
P{KK109052}VIE-260B (TfAP-2KK109052)	Vienna Drosophila Resource Center (VDRC): v101552	(Dietzl et al. 2007)
w[1118]; P{w[+mC]=UAS-Dcr-2.D}10	BDSC: 24651	(Dietzl et al. 2007)
dsf^{Del}	Troy Shirangi	(Duckhorn et al. 2022)
y[1] w[*]; Mi{y[+mDint2]=MIC}fru[MI05459]	BDSC: 42086	(Nagarkar-Jaiswal et al. 2015)
w[1118]; P{y[+t7.7] w[+mC]=R55E01-GAL4.DBD}attP2	BDSC: 69662	(Dionne et al. 2018)

w[1118]; P{y[+t7.7] w[+mC]=R29F12-p65.AD}attP40; P{y[+t7.7] w[+mC]=R24A03-GAL4.DBD}attP2	BDSC: 86777	(Dionne et al. 2018)
pdm3-DBD	Gift from David Chen	unpublished
br-Z4	Haluk Lacin	Allen, Neville, Lacin, and Goodwin 2025, submitted
fru-flp	Barry Dickson	(J. Y. Yu et al. 2010)

Antibodies

Reagent	**Source**	**Identifier**
Anti-GFP (rabbit polyclonal)	Fisher	Cat# A11122
Anti-GFP (chicken polyclonal)	Cai Lab	N/A
Anti-RFP (rat monoclonal)	chromtek	5f8-150
Anti-Broad-Core (mouse Monoclonal)	Developmental Studies Hybridoma Bank	25E9.D7
Anti-Pdm3 (Rat)	Desplan Lab	(Özel et al. 2022)
Anti-TfAP-2 (guinea pig)	Desplan Lab	(Konstantinides et al. 2022)
Anti-Mamo (guinea pig)	Desplan Lab	(Rossi and Desplan 2020)
Anti-GABA (rabbit	Sigma	A2052
Alexa 488 anti-chicken (goat polyclonal)	Fisher	A-11039
Alexa 488 anti-rabbit (goat polyclonal)	Fisher	A-11034
Alexa 568 anti-rat (goat polyclonal)	Fisher	A-11077
Alexa 568 anti-guinea pig (goat polyclonal)	Fisher	A-11075
Alexa 647 anti-rat (goat polyclonal)	Fisher	A48265
Alexa 647 anti-mouse (goat polyclonal)	Fisher	A-21236
Alexa 647 anti-rabbit (goat polyclonal)	Fisher	A-21244

Oligonucleotides

Oligonucleotide	**Source**	**Identifier**
Drosophila fru HCR v3.0 probe set (B1)	Molecular Instruments	Lot#RTD524
Drosophila grim HCR v3.0 probe set (B2)	Molecular Instruments	Lot#PRQ961
Drosophila TfAP-2 HCR v3.0 probe set (B5)	Molecular Instruments	Lot#RTI749
Drosophila fd59A HCR v3.0 probe set (B4)	Molecular Instruments	Lot#RTI748
Drosophila Fer1 HCR v3.0 probe set (B2)	Molecular Instruments	Lot# PIO665

Drosophila pdm3 HCR v3.0 probe set (B4)	Molecular Instruments	Lot#RTL279
B1 546 HCR Amplifier	Molecular Instruments	N/A
B2 647 HCR Amplifier	Molecular Instruments	N/A
B4 488 HCR Amplifier	Molecular Instruments	N/A
B5 647 HCR Amplifier	Molecular Instruments	N/A
B4 647 HCR Amplifier	Molecular Instruments	N/A
CTTCGTTAGATGCCAGGACTAGCA (Fer1-T2A-GAL4_3'gRNA_sense)	Integrated DNA Technologies (IDT)	N/A
AAACTGCTAGTCCTGGCATCTAAC (Fer1-T2A-GAL4_3'gRNA_antisense)	Integrated DNA Technologies (IDT)	N/A
CTTCGCTGTTGTTGTACAGCGGCA (Fer1-T2A-GAL4_5'gRNA_sense)	Integrated DNA Technologies (IDT)	N/A
AAACTGCCGCTGTACAACAACAGC (Fer1-T2A-GAL4_5'gRNA_antisense)	Integrated DNA Technologies (IDT)	N/A
TTCGTAGGCGTACTTCACATCT (for genotyping Fer1-T2A-GAL4, in Fer1 homology arm)	Integrated DNA Technologies (IDT)	N/A
AGAGTAGCGACACTCCCAGT (for genotyping Fer1-T2A-GAL4, in GAL4)	Integrated DNA Technologies (IDT)	N/A

Software and algorithms

Reagent	**Source**	**Identifier/ Citation**
FIJI	https://imagej.net/software/fiji/downloads	(Schindelin et al. 2012)
R	https://www.R-project.org/	(R Foundation for Statistical Computing, 2023)
R package Seurat	https://satijalab.org/seurat/	(Hao et al. 2024)
R package scCustomize	https://samuel-marsh.github.io/scCustomize/index.html	(Samuel Marsh et al. 2024)
R package Clustree	https://lazappi.github.io/clustree/	(Zappia and Oshlack 2018)
R package UCell	https://github.com/carmonalab/UCell	(Andreatta and Carmona 2021)
R package (RColorBrewer)	https://CRAN.R-project.org/package=RColorBrewer	(Neuwirth 2022)
R package (viridisLite)	https://cran.r-project.org/web/packages/viridis/index.html	(Garnier et al. 2023)
R package (tidyverse)	https://tidyverse.tidyverse.org	(Wickham et al. 2019)

Plasmids

Plasmid	**Source**	**Identifier**
pBS-KS-attB1-2-GT-SA-mCherry-SV40	Drosophila Genomics Resource Center	(DGRC Stock 1324 ; https://dgrc.bio.indiana.edu//stock/1324; RRID:DGRC_1324)

pBS_KS_attB2_SA(0)_T2AGAL4	Addgene	a gift from Herman Dierick (Addgene plasmid # 125211 ; http://n2t.net/addgene:125211 ; RRID:Addgene_125211)
pU6-BbsI-chiRNA	Addgene	pU6-BbsI-chiRNA was a gift from Melissa Harrison & Kate O'Connor-Giles & Jill Wildonger (Addgene plasmid # 45946 ; http://n2t.net/addgene:45946 ; RRID:Addgene_45946)

Chemicals, peptides, and recombinant proteins

Reagent	**Source**	**Identifier**
Paraformaldehyde	EMS	15710
Normal Goat Serum	MP biomedicals	8642921
Triton	Sigma	X100
Sodium chloride NaCl	Sigma	S7653
Potassium chloride KCl	Fisher	P217-500
Calcium chloride CaCl2*2H2O	Fisher	C70-500
Magnesium chloride MgCl2*6H2O	Sigma	M2670
HEPES sodium salt	Sigma	H7006
Trehalose	Sigma	T9531
Sucrose	Sigma	84097
Sodium bicarbonate NaHCO3	Fisher	S233-500
Sodium phosphate NaH2PO4*H2O	Fisher	S369-500
Propyl gallate	Sigma	2370
SlowFade™ Glass Soft-set Antifade	Fisher	S36917
UltraPure™ SSC, 20X	Invitrogen	15557044
Schneider's Insect Medium	Sigma	S0146
Collagenase from *Clostridium histolyticum*	Sigma	C0130
10X PBS Gibco	Fisher	70-011-044
Bovine Serum Albumin	Sigma	A9085
Tween-20	Sigma	P1379
invitrogen ultrapure DNase/RNase-free distilled water	Fisher	10977015
Normal Goat Serum 50 mL	abcam	ab7481
Dextran, Texas Red™, 3000 MW, Lysine Fixable	ThermoFisher	D3328

Other

Reagent	**Source**	**Identifier**
Fly food	Lab Express, Ann Arbor MI	“B” Food

Critical commercial assays

Reagent	**Source**	**Identifier**

HCR RNA-FISH Bundle	Molecular Instruments	N/A

Flow Cytometry: Flow cytometry to sort GFP-positive neurons from pupal brains was performed similarly to adult brains (Brovkina et al., 2021): Dissections of fly brains were done in Schneider's+1% BSA for up to one hour. Optic lobes were removed for the 48hrAPF time points. After dissections, Collagenase was added to the brains at a concentration of 2mg/ml in Schneider's+1% BSA then placed at 37C for 12 minutes (versus 20 minutes for adult brains). Afterwards, we did a manual dissociation by pipetting the brains up and down at least 30 times, then spun down the cells at 300g for 5 minutes. We removed the supernatant, then resuspended the pellet in 200ul of PBS + 0.1% BSA, passed it through a cell strainer cap, and spun it down briefly to collect cell suspension at the bottom of the tube. We added 50ng/mL of DAPI to our sample and then sorted them on a FACSAria III (University of Michigan BRCF Flow Cytometry Core) into a PBS + 1% BSA cushion. We pretreated plasticware including tips and eppendorf tubes with PBS + 1% BSA to prevent cells from sticking to the plastic. During flow cytometry, dead and dying cells were excluded using DAPI signal, and forward scatter and side scatter measurements were used to gate single cells. Scatter profiles consistent with somata (rather than neurite fragments) were determined by back-gating on DAPI. Using our dissociation methods, ~70–90% of singlets appeared viable (DAPI-low) for both time points. Because the cells were to be analyzed using single cell sequencing, we set our gates generously (i.e. tolerated sorting false positive cells so as to capture all true positives). With these generous gates, 9-13% of these viable cells were gated as GFP+ for our 48hrAPF time points, and ~2% for 12hrAPF. During sorting, we made two adjustments to protect the fly primary cells, which were very delicate—we disabled agitation of the sample tube, and sorted using the "large nozzle," (100µm, i.e. using larger droplet size and lower pressure).

scRNA-seq quality control metrics: We prepared 6 libraries using the lineage labelling strategy: 2 replicates at 48hrAPF, 2 replicates at 48h APF with apoptosis blocked, and 2 replicates at 12h APF with apoptosis blocked. Potential doublets and low-quality cells were filtered out by discarding cells that didn't express lexAop-GFP, lexAop-p35 or LexA-p65, cells with >50000 UMIs, cells with < 1000 unique features and cells with >5% mitochondrial genes. Features corresponded to genes that were expressed in at least one cell across libraries. After filtering we had a total of 43650 cells.

scRNA-seq clustering and integration of libraries: We merged all the libraries and used the Seurat package (Seurat V5) (Hao et al. 2024) to cluster and integrate our datasets and to visualize our clusters across conditions (+/- p35) and timepoints (12 vs 48hrAPF). To do this, we normalized gene expression using the NormalizeData function (LogNormalize method). Rather than finding and using the most highly variable genes for the subsequent steps, we used a list of 628 transcription factors from FlyBase – 609 of which were expressed in our cells. We then scaled our data (ScaleData) while regressing out mitochondrial gene expression (percent.mito) and sequencing depth (nCount_RNA). We then ran principal component analysis using the scaled expression of our 609 transcription factors (RunPCA) otherwise using default parameters. For clustering and visualizing, we used default parameters, including 50 principal components based on an ElbowPlot (0-200) (FindClusters, FindNeighbors and RunUMAP). We then integrated our datasets (IntegrateLayers) using Harmony Integration and ran the clustering (FindClusters,

FindNeighbors and RunUMAP) as we just described above to get an idea of the cell types and cell type diversity that existed in our dataset.

To enrich for non-MB Type I hemilineages, we removed Kenyon cells, glia and 12hrAPF-specific clusters we found to be optic lobe neurons or progenitor cells (Figure S1C-D): In our top-level clustering, Cluster 5 contained Kenyon cells based on the expression of *Mef2*, *ey* and *dac.* Clusters 0 and 16 were glia based on the expression of *repo.* Cluster 0 primarily contained cells from a single library (low quality cells), so we removed it. 7 clusters (11, 39, 18, 21, 38, 26, 40) were specific to the 12hrAPF time point and were enriched for *scro* but depleted of *Imp* and *dati* (Davie et al. 2018) indicating they are optic lobe neurons. (At 48h APF, we removed optic lobes during our dissections; at 12h APF, the optic lobes have not yet separated from the central brain and are thus present during our sorting.) 14, 41 and 23 expressed *dpn* or *dap* and were presumed to be progenitor cells and removed. Some of these cell types are truly labeled by our recombination-based strategy (progenitors, glia deriving from Type I lineages, sporadic clone induction in KC lineages). Others are false positives due to a combination of our generous gating and their prevalence. After filtering, we retained a total of 31091 neurons (17007 cells from 48hrAPF and 14084 cells from 12hrAPF). Figure 1 supplement has the breakdown of how many cells come from each library (Figure S1E). To generate the final clustering map, we used for biological analyses, we re-ran the workflow above, except that after integrating the datasets, we used a resolution of 1.6 in FindClusters determined using ClusTree (Zappia and Oshlack 2018). This produced relative stabilization of 52 clusters that we assign as postmitotic neurons originating from central brain, Type I lineages.

As we describe in the results text, we hypothesize that these clusters mainly corresponded to hemilineages, with larger clusters representing hemilineages always labeled by our lineage trace, and smaller clusters representing hemilineages that were labeled more rarely. That said, as we worked back and forth between the transcriptional to histological points of view, we observed that there was no single clustering resolution that perfectly reflected hemilineage relationships: At lower resolution, some clusters contained multiple hemilineages (e.g. anterodorsal and lateral olfactory projection neuron hemilineages), while at higher resolution, some hemilineages split into more than one cluster along the birth order axis. We chose a resolution that kept most hemilineages unified and manually split some of our clusters, as shown in Figure S1 (I-J). For example, cluster 1 contained the *DAT*+ CREa1A neurons, which express *Scro*, *dmrt99B*, *erm*, *D, Lim1*, *hth, SoxN, CG9932* and *Fer2*, along with other cells that strongly shared *Fer2, Scro, D,* and *hth* but lacked DAT and expressed *Gad1* and appeared to be destined to apoptose based on expression of *grim*. This suggested they are a hemilineage that typically undergoes apoptosis, which we suspect to be SMPad1B. In this case, we called the *DAT*+ neurons as CREa1A, and referred to the rest of the cells as "cluster 1," as we have not verified their match to SMPad1B. We also manually split adPNs and lPNs based on the expression of *acj6,* which is specific to adPNs.

Subclustering and integration of CREa1B cells: Subclustering was performed using the standard Seurat workflow: gene counts were normalized (function: NormalizeData); 2000 highly-variable genes (FindVariableFeatures) were scaled and used for PCA (functions: ScaleData/RunPCA); first 50 principle components were used for clustering (functions: FindNeighbors/FindClusters) and UMAP projections (function: RunUMAP). For integration we used the standard integration workflow of Seurat 5 using Anchor-based CCA integration to identify shared cell types across conditions (+/- p35) and time (12hr and 48hr APF). It works by correcting the previously identified

PCA coordinates and these corrected coordinates are for clustering (functions: FindNeighbors/FindClusters, resolution = 0.4, 7 clusters) and UMAP projections (function: RunUMAP) (Hao et al. 2024).
Proportion of mAL types in males vs females was calculated by dividing the number of *pdm3* or *br* expressing mALs by the total number of fru neurons for each condition (+/-p35).

Re-clustering of (Davie et al. 2018) data: The Davie_Janssens_Koldere_et_al_2018_AdultBrain.loom loom object was downloaded from the Aerts Lab website. The reclustering was performed using the standard Seurat workflow based on transcription factor expression rather than variable gene expression. A list of 628 transcription factors from FlyBase was used – 555 of which were expressed in the Davie dataset (although this could be higher and due to nomenclature differences). We then scaled the data (ScaleData) while regressing out mitochondrial gene expression (percent.mito) and sequencing depth (nCount_RNA). We then ran principal component analysis using the scaled expression of these 555 transcription factors (RunPCA) otherwise using default parameters. For clustering and visualizing, we used default parameters, including 50 principal components (FindClusters, FindNeighbors and RunUMAP).

Differentially expressed gene analyses: All differentially expressed gene analyses were done using the FindMarkers function using default parameters. Afterwards the differentially genes were filtered for any non-coding RNAs besides *lncRNA:roX1* and *lncRNA:roX2*, mitochondrial genes, transposable elements, ribosomal proteins and mod(mdg4) trans-spliced precursors. Plots were made using the ggplot2 package. CREa1B, CREa1A, cluster 1, ALad1B (adPNs) and ALl1B (lPNs) marker genes were determined by comparing each of those clusters to all other clusters in the dataset. In the case of CREa1B, clusters were split by time point first, then marker genes were found as described above.

Categorizing transcription factor expression: Computational approach/ FindAllMarkers: For the differential gene expression analyses, we used the FindAllMarkers function from Seurat (Hao et al. 2024), using the default Wilcoxon Rank Sum test on log-normalized feature counts for our 52 clusters before splitting cluster 1 and the projection neuron cluster. We selected for transcription factors that had a minimum percentage difference (min.diff.pct) between the two populations of 50% because we were looking for positive marker transcription factors for our clusters, resulting in 103 transcription factors.

Categorizing transcription factor expression: Manual categorization of transcription factor expression: For manual categorization of transcription factor expression, we used Seurat "featureplots" to display the expression of the 609 FlyBase TFs that were expressed in at least one cell in our integrated dataset; we split our dataset by timepoint in order to discern maturation-based changes in TF expression. We blinded ourselves to gene names, and then categorized each expression pattern as "lineage" (expression in one or more, but not all, whole clusters) "order" (expression in subsets of cells within each cluster), or "maturation" (broad expression, varying across time points). Transcription factors that did not fit into these three simple categories were categorized as either "sparse" (likely low but general expression, positive cells scattered), "everywhere" (pan-neuronal, universal transcription factors) "weird" (described in the results, usually a combination of the other axes), "NA" (non-expressed), and rarely, multiple labels. Overall, we found 124 putative hemilineage transcription factors, of which 91 had cluster-defining

and cluster-specific expression without varying over other axes. We identified 35 transcription factors we hypothesize reflect birth order. Our manual descriptions of the expression patterns of each TF are provided in Supplemental Table 2. Four transcription factors were overlapping between these lists (*svp*, *luna*, *RunxA* and *Dbx*) and so we removed them from the list of transcription factors we hypothesize reflect birth order and manually added chinmo and hb to that list of TFs, due to their known roles in temporal patterning and after manual re-inspection. This resulted in 33 TFs we refer to as "birth order TFs". We focused our spatial TF analyses on the 91 TFs with simple cluster-defining expression, as described above, and we refer to them as "hemilineage TFs".

Lineage variability and temporal dynamicity scores: We also computationally assigned each gene in our dataset a lineage variability score and a temporal dynamicity score. These scores were calculated using code generously shared by Saumya Jain and implemented similarly as in (Jain et al. 2022): We converted our cells into pseudo-bulk RNA-seq datasets based on their cluster identity and time (cluster 1 12hrAPF, cluster 1 48hrAPF…etc) by aggregating the expression of counts according to cluster and time (AggregateExpression) (Hao et al. 2024). The lineage variability score was calculated by determining the variance in gene expression across lineages within either time point, taking the maximum of those two scores, and then normalizing by the average expression across cell types at the relevant time point. The temporal dynamicity score was calculated by taking the absolute difference between our 12hr and 48hr timepoints for each of our hemilineages/ clusters where the gene was expressed, and the averaged value across clusters was then normalized by the average of the peak expression. Both scores had their mean centered to 0 and were transformed to the natural log scale for visualization.

Heatmaps: Heatmaps were made using the pheatmap package in R in figures 3 and 4. (Kolde R (2018). pheatmap: Pretty Heatmaps. R package version 1.0.12, https://github.com/raivokolde/pheatmap.)

We identified protein domains enriched within the 91 hemilineage TFs and 33 birth order TFs using DAVID Bioinformatics Functional Annotation Tool and FlyBase (Huang, Sherman, and Lempicki 2009; Sherman et al. 2022).

We used the UCell package (Andreatta and Carmona 2021) to calculate the gene set enrichment scores at single-cell level of the following genes: 1. *VAChT*, *DAT*, *VGlut*, *Gad1*, 2. *fru* 3. *rpr, skl* and *grim* to assign our pseudobulk clusters a neurotransmitter identity, whether it's sexually-dimorphic based on *fru* expression, and to an apoptosis score. The ranking in UCell uses the Mann-Whitney U statistic.

Variance across vs within clusters vs across time: We calculated the variance in expression for each transcription factor across our pseudobulk clusters grouped by either cluster or time. Median cluster variance was calculated by finding the variance in expression for each transcription factor for each cluster and taking the median value for each transcription factor.

fruMiMIC[mcherry] (fru-mCherry): The *fru*MiMIC[mcherry] flies were made via recombinase-mediated cassette exchange (RMCE) performed by Rainbow Transgenic Flies Inc. with the pBS-KS-attB1-2-GT-SA-mcherry-SV40 vector ordered from the Drosophila Genomics Resource Center (DGRC Stock Number: 1324) (Venken et al. 2011). The DNA was prepared with a Qiagen

Plasmid Midi Kit and injected into the original *fru*[MI05459] line (BDSC: 42086). Transformants were crossed to yw double balancer flies and were screened for loss of y+ over the third balancer. As the swap-in allele can incorporate in either direction, we screened F1 progeny of animals positive for loss of the original MiMIC allele for *fru*-mCherry expression using our 2P microscope. (mCherry has a poor 2p excitation profile, but we captured the edge of its 1p excitation using ~700nm illumination.)

Fer1-T2A-Gal4: The Fer1-T2A-GAL4 construct was made using CRISPR/Cas9 HDR as previously described in (Xiao, Yuan, and Yadlapalli 2022). The donor cassette was designed so as to have ~1kb homology arms flanking the stop codon (5' PAM silently mutated, 3' PAM deleted) with the T2A-Gal4 sequence, taken from addgene#125211 (Gnerer, Venken, and Dierick 2015), immediately preceding the stop codon. The donor construct was synthesized and cloned into pBluescript II SK(-) by GENEWIZ from Azenta Life Sciences. Two Fer1 gRNA sequences were generated, as listed in the Oligonucleotides section, and each was synthesized as overlapping primers and annealed to generate dsDNA with BbsI overhangs. Each guide (5' and 3') was cloned into pU6-BbsI-chiRNA, generating 5' and 3' Fer1 gRNA plasmids. These two plasmids, together with the homology-directed repair donor, were cleaned and injected into *y,sc,v; nos-Cas9; +/+* (X. Ren et al. 2013) by Rainbow Transgenic Flies Inc. Injected flies were crossed to double balancers and their progeny were screened by PCR genotyping of amputated legs using the primers listed in the Oligonucleotides section.

Brain dissection and two photon imaging: Brains were dissected in external saline (108 mM NaCl, 5 mM KCl, 2 mM CaCl2, 8.2 mM MgCl2, 4 mM NaHCO3, 1 mM NaH2PO4, 5 mM trehalose, 10 mM sucrose, 5 mM HEPES pH7.5, osmolarity adjusted to 265 mOsm). For two-photon imaging, brains were then transferred fresh to 35mm imaging dishes and pinned to sylgard squares with tungsten wire. Ex vivo two photon imaging was performed on a Bruker Investigator using a 1.0 NA, 20x, water-dipping objective. Stacks were collected along the anterior-posterior axis with 1 micrometer spacing in Z and variable resolution in X/Y.

Immunostaining and confocal microscopy: For immunostaining, after dissections brains were transferred to paraformaldehyde in PBS. Brains were fixed overnight at 4C in 1% PFA in PBS or for 25 minutes at room temperature in 4% PFA in PBS. In general, the 4% PFA method preserves cellular structures better, while the 1% PFA method allows better antibody penetration. After same-day (4%) or overnight (1%) fixation, brains were washed 3 times in PBS supplemented with 0.1% Triton-X-100 on a shaker at room temperature, blocked for at least 1 hour in PBS, 0.1% triton, 4% Normal Goat Serum, and then incubated for at least two overnights in primary antibody solution, diluted in PBS, 0.1% triton, 4% Normal Goat Serum. Primary antibody was washed 3x in PBS supplemented with 0.1% triton-x-100 on a shaker at room temperature, then brains were incubated in secondary antibodies for at least two overnights, diluted in PBS, 0.1% triton, 4% Normal Goat Serum. DAPI (1 microgram/mL) was included in secondary antibody mixes. Antibodies and concentrations can be found in the Key Resources Table

Brains were mounted in 1x PBS, 90% glycerol supplemented with propyl gallate or SlowFade mounting medium in binder reinforcement stickers sandwiched between two coverslips. Samples were stored at 4C in the dark prior to imaging. The coverslip sandwiches were taped to slides, allowing us to perform confocal imaging on one side of the brain and then flip over the sandwich

to allow a clear view of the other side of the brain. Scanning confocal stacks were collected along the anterior-posterior axis on a Leica SP8 with 1 micrometer spacing in Z and ~150nm axial pixel size, using a 40x 1.3 NA oil immersion objective. Z dimension corresponds to anterior to posterior dimension of the central brain.

For Figure 5I Left and Right, brains were stained and imaged as described in (Diamandi et al. 2024).

IHC with DPX mounting: In some cases, we sought to improve tissue clarity in IHC experiments using DPX mounting. To do this, brains were dissected in dissection saline, and then fixed in cold 4% PFA in PBS for 25min. Following fixation, brains were washed three times with 0.1% PBST (PBS containing 0.1% Triton X-100), then mounted onto a poly-L-lysine-coated coverslip. Blocking, primary antibody incubation and secondary antibody incubation were performed as described above. After secondary antibody incubation, the samples were washed with 0.1% PBST for three times, then subsequently post-fixed with 4% PFA for 2hrs at room temperature. After post-fixation, PFA was removed, and samples were washed four times with 0.1% PBST. The tissues were then dehydrated through a graded ethanol series (30%, 50%, 75%, 95%, and 2 × 100%), with each step lasting 5 minutes. This was followed by three washes in xylene (5min each). Finally, samples were mounted onto glass slides using DPX mounting medium. Mounted slides were air-dried for at least 2 days at room temperature before confocal imaging and stored at room temperature thereafter.

HCR RNA FISH: RNA fluorescent *in situ* hybridization (RNA-FISH) experiments were done as described by Ferreira et al., 2021 using Molecular Instruments HCR probe-sets, hairpins and reagents (Choi et al. 2018; A. G. Ferreira, Sieriebriennikov, and Whitbeck 2021). Brains were dissected in Schneider's Drosophila Medium and fixed in cold 4% paraformaldehyde in PBS for 20 minutes at room temperature. Brains were rinsed 3x at room temperature in PBS supplemented with 1% triton-x-100 at room temperature then washed 3x with PBS supplemented with 1% triton-x-100 at room temperature. Samples were pre-hybridized in prewarmed Probe Hybridization Buffer (Molecular Instruments™) for 10 minutes at 37C and then incubated with HCR probes in Probe Hybridization Buffer overnight at 37C. The next day, they were washed with pre-heated Probe Wash Buffer (Molecular Instruments™) then washed 2 times in 5xSSCT (5X sodium chloride sodium citrate supplemented with 0.1% Tween-20). Samples were then preamplified in Amplification Buffer (Molecular Instruments™) for 10-30 minutes at room temperature and then incubated with snap-cooled HCR hairpins (95C for 90 seconds and then placed in the dark at room temperature for at least 30 minutes) in the dark overnight at room temperature. Before washing the brains, 300ul 5XSSCT was added to the samples to make the solution less viscous. The brains were then washed three times at room temperature first in 5XSSCT, then in Probe Wash Buffer (Molecular Instruments™) and then again in 5XSSCT. The brains were then rinsed one in Nuclease-Free PBS to remove any detergent and then were mounted in 1x PBS, 90% glycerol supplemented with propyl gallate and imaged as described above.

Combined RNA FISH and Immunohistochemistry: RNA fluorescent *in situ* hybridization (RNA-FISH) and Immunohistochemistry experiments were done as described by Schwarzkopf et al., 2021 using Molecular Instruments HCR probe-sets, hairpins and reagents (Schwarzkopf et al. 2021). The protein detection stage was first, with care to avoid introducing RNases into the solutions. Brains were dissected in external saline (108 mM NaCl, 5 mM KCl, 2 mM CaCl2, 8.2

mM MgCl2, 4 mM NaHCO3, 1 mM NaH2PO4, 5 mM trehalose, 10 mM sucrose, 5 mM HEPES pH7.5, osmolarity adjusted to 265 mOsm) and fixed in 4% paraformaldehyde in PBS for 25 minutes at room temperature. Brains were then washed 3x with PBS supplemented with 0.1% triton-x-100 at room temperature, blocked in Antibody Buffer (Molecular Instruments) at 4C for ~4hrs, and then incubated overnight at 4C in primary antibody solution in Antibody Buffer (Molecular Instruments). Samples were then washed 4X in PBS supplemented with 0.1% triton-x-100 at room temperature and incubated in secondary antibody solution made in Antibody Buffer (Molecular Instruments). For some experiments we used the Molecular Instruments initiator labelled secondary antibody to amplify GFP signal (Donkey Anti-Rabbit-B4 for use with amplifier B4) and in other cases we used standard secondary antibodies (Goat Anti-Rabbit-488). Samples were incubated at room temperature for 3 hours then were washed 5X in PBS supplemented with 0.1% triton-x-100 then 1X in 5XSSCT both at room temperature. Samples were then preamplified in Amplification Buffer (Molecular Instruments™) for 10-30 minutes at room temperature and then incubated with snap-cooled HCR hairpins (95C for 90 seconds and then placed in the dark at room temperature for at least 30 minutes) in the dark overnight at room temperature. The brains were then washed in 5XSSCT at room temperature for (1) 2X5min (2) 2X30min and (3) 1X5min. The samples were then mounted as described above.

Dye filling of mAL neurons: Dye filling of mAL neurons was performed as previously described in (Clowney et al., 2015; Ruta et al., 2010). Dye filling electrodes were pulled using a Brown/Flaming puller (Sutter Instruments) and were guided to the mAL axonal tract using *fru*-GFP. Voltage pulses (50-V pulses, 0.5 ms) were used to electroporate dye into the cells.

Image analysis & statistical considerations: The sexes were separated across experimental conditions because mAL neurons are sexually dimorphic. To count cell populations, we used genetically encoded fluorescence or antibody staining as indicated. We counted labeled somata in every third slice in the stack (every third micron along the A-P axis), with reference to DAPI to distinguish individual cells from one another. Effect of mutations on axons and dendrites were done in a binary fashion due to the overt changes on brain structures induced by our manipulations, which also made it difficult for the researchers performing quantification to be blinded to experimental conditions. However, analysis was performed blind to the goals of the experiment when possible.

References

A. G. Ferreira, Amanda, Bogdan Sieriebriennikov, and Hunter Whitbeck. 2021. "HCR RNA-FISH Protocol for the Whole-Mount Brains ofDrosophila and Other Insects V1." https://doi.org/10.17504/protocols.io.bzh5p386.

Allen, Aaron M, Megan C Neville, Sebastian Birtles, Vincent Croset, Christoph Daniel Treiber, Scott Waddell, and Stephen F Goodwin. 2020. "A Single-Cell Transcriptomic Atlas of the Adult Drosophila Ventral Nerve Cord." *eLife* 9 (April):e54074. https://doi.org/10.7554/eLife.54074.

Andreatta, Massimo, and Santiago J. Carmona. 2021. "UCell: Robust and Scalable Single-Cell Gene Signature Scoring." *Computational and Structural Biotechnology Journal* 19:3796–98. https://doi.org/10.1016/j.csbj.2021.06.043.

Arlotta, Paola, and Oliver Hobert. 2015. "Homeotic Transformations of Neuronal Cell Identities." *Trends in Neurosciences* 38 (12): 751–62. https://doi.org/10.1016/j.tins.2015.10.005.

Awasaki, Takeshi, Chih-Fei Kao, Ying-Jou Lee, Ching-Po Yang, Yaling Huang, Barret D Pfeiffer, Haojiang Luan, et al. 2014. "Making Drosophila Lineage–Restricted Drivers via Patterned Recombination in Neuroblasts." *Nature Neuroscience* 17 (4): 631–37. https://doi.org/10.1038/nn.3654.

Bailey, Peter J., Joanna M. Klos, Elisabet Andersson, Mattias Karlén, Magdalena Källström, Jasmina Ponjavic, Jonas Muhr, Boris Lenhard, Albin Sandelin, and Johan Ericson. 2006. "A Global Genomic Transcriptional Code Associated with CNS-Expressed Genes." *Experimental Cell Research* 312 (16): 3108–19. https://doi.org/10.1016/j.yexcr.2006.06.017.

Bayraktar, Omer Ali, and Chris Q. Doe. 2013. "Combinatorial Temporal Patterning in Progenitors Expands Neural Diversity." *Nature* 498 (7455): 449–55. https://doi.org/10.1038/nature12266.

Bello-Rojas, Saul, and Martha W Bagnall. 2022. "Clonally Related, Notch-Differentiated Spinal Neurons Integrate into Distinct Circuits." *eLife* 11 (December):e83680. https://doi.org/10.7554/eLife.83680.

Bonchuk, Artem, Stepan Denisov, Pavel Georgiev, and Oksana Maksimenko. 2011. "Drosophila BTB/POZ Domains of 'Ttk Group' Can Form Multimers and Selectively Interact with Each Other." *Journal of Molecular Biology* 412 (3): 423–36. https://doi.org/10.1016/j.jmb.2011.07.052.

Bou Dib, Peter, Bettina Gnägi, Fiona Daly, Virginie Sabado, Damla Tas, Dominique A. Glauser, Peter Meister, and Emi Nagoshi. 2014. "A Conserved Role for P48 Homologs in Protecting Dopaminergic Neurons from Oxidative Stress." Edited by Bingwei Lu. *PLoS Genetics* 10 (10): e1004718. https://doi.org/10.1371/journal.pgen.1004718.

Briscoe, James, Alessandra Pierani, Thomas M Jessell, and Johan Ericson. 2000. "A Homeodomain Protein Code Specifies Progenitor Cell Identity and Neuronal Fate in the Ventral Neural Tube." *Cell* 101 (4): 435–45. https://doi.org/10.1016/S0092-8674(00)80853-3.

Brovkina, Margarita V., Rachel Duffié, Abbigayl E. C. Burtis, and E. Josephine Clowney. 2021. "Fruitless Decommissions Regulatory Elements to Implement Cell-Type-Specific Neuronal Masculinization." Edited by Claude Desplan. *PLOS Genetics* 17 (2): e1009338. https://doi.org/10.1371/journal.pgen.1009338.

Bürglin, Thomas R., and Markus Affolter. 2016. "Homeodomain Proteins: An Update."

Chromosoma 125 (3): 497–521. https://doi.org/10.1007/s00412-015-0543-8.
Cachero, Sebastian, Aaron D. Ostrovsky, Jai Y. Yu, Barry J. Dickson, and Gregory S.X.E. Jefferis. 2010. "Sexual Dimorphism in the Fly Brain." *Current Biology* 20 (18): 1589–1601. https://doi.org/10.1016/j.cub.2010.07.045.
Chen, Yu-Chieh David, Yen-Chung Chen, Raghuvanshi Rajesh, Nathalie Shoji, Maisha Jacy, Haluk Lacin, Ted Erclik, and Claude Desplan. 2023. "Using Single-Cell RNA Sequencing to Generate Predictive Cell-Type-Specific Split-GAL4 Reagents throughout Development." *Proceedings of the National Academy of Sciences* 120 (32): e2307451120. https://doi.org/10.1073/pnas.2307451120.
Chen, Yu-Chieh David, and Anupama Dahanukar. 2020. "Recent Advances in the Genetic Basis of Taste Detection in Drosophila." *Cellular and Molecular Life Sciences* 77 (6): 1087–1101. https://doi.org/10.1007/s00018-019-03320-0.
Choi, Harry M. T., Maayan Schwarzkopf, Mark E. Fornace, Aneesh Acharya, Georgios Artavanis, Johannes Stegmaier, Alexandre Cunha, and Niles A. Pierce. 2018. "Third-Generation *in Situ* Hybridization Chain Reaction: Multiplexed, Quantitative, Sensitive, Versatile, Robust." *Development* 145 (12): dev165753. https://doi.org/10.1242/dev.165753.
Clark, Brian S., Genevieve L. Stein-O'Brien, Fion Shiau, Gabrielle H. Cannon, Emily Davis-Marcisak, Thomas Sherman, Clayton P. Santiago, et al. 2019. "Single-Cell RNA-Seq Analysis of Retinal Development Identifies NFI Factors as Regulating Mitotic Exit and Late-Born Cell Specification." *Neuron* 102 (6): 1111-1126.e5. https://doi.org/10.1016/j.neuron.2019.04.010.
Clowney, E. Josephine, Shinya Iguchi, Jennifer J. Bussell, Elias Scheer, and Vanessa Ruta. 2015. "Multimodal Chemosensory Circuits Controlling Male Courtship in Drosophila." *Neuron* 87 (5): 1036–49. https://doi.org/10.1016/j.neuron.2015.07.025.
Davie, Kristofer, Jasper Janssens, Duygu Koldere, Maxime De Waegeneer, Uli Pech, Łukasz Kreft, Sara Aibar, et al. 2018. "A Single-Cell Transcriptome Atlas of the Aging Drosophila Brain." *Cell* 174 (4): 982-998.e20. https://doi.org/10.1016/j.cell.2018.05.057.
Deere, Julia U, Arvin A Sarkissian, Meifeng Yang, Hannah A Uttley, Nicole Martinez Santana, Lam Nguyen, Kaushiki Ravi, and Anita V Devineni. 2023. "Selective Integration of Diverse Taste Inputs within a Single Taste Modality." *eLife* 12 (January):e84856. https://doi.org/10.7554/eLife.84856.
Demir, Ebru, and Barry J. Dickson. 2005. "Fruitless Splicing Specifies Male Courtship Behavior in Drosophila." *Cell* 121 (5): 785–94. https://doi.org/10.1016/j.cell.2005.04.027.
Diamandi, Julia A., Julia C. Duckhorn, Kara E. Miller, Mason Weinstock, Sofia Leone, Micaela R. Murphy, and Troy R. Shirangi. 2024. "Developmental Remodeling Repurposes Larval Neurons for Sexual Behaviors in Adult Drosophila." *Current Biology* 34 (6): 1183-1193.e3. https://doi.org/10.1016/j.cub.2024.01.065.
Diao, Fengqiu, Holly Ironfield, Haojiang Luan, Feici Diao, William C. Shropshire, John Ewer, Elizabeth Marr, Christopher J. Potter, Matthias Landgraf, and Benjamin H. White. 2015. "Plug-and-Play Genetic Access to Drosophila Cell Types Using Exchangeable Exon Cassettes." *Cell Reports* 10 (8): 1410–21. https://doi.org/10.1016/j.celrep.2015.01.059.
Dietzl, Georg, Doris Chen, Frank Schnorrer, Kuan-Chung Su, Yulia Barinova, Michaela Fellner, Beate Gasser, et al. 2007. "A Genome-Wide Transgenic RNAi Library for Conditional Gene Inactivation in Drosophila." *Nature* 448 (7150): 151–56. https://doi.org/10.1038/nature05954.

Dionne, Heather, Karen L Hibbard, Amanda Cavallaro, Jui-Chun Kao, and Gerald M Rubin. 2018. "Genetic Reagents for Making Split-GAL4 Lines in *Drosophila*." *Genetics* 209 (1): 31–35. https://doi.org/10.1534/genetics.118.300682.

Doe, Chris Q. 2017. "Temporal Patterning in the *Drosophila* CNS." *Annual Review of Cell and Developmental Biology* 33 (1): 219–40. https://doi.org/10.1146/annurev-cellbio-111315-125210.

Dorkenwald, Sven, Arie Matsliah, Amy R. Sterling, Philipp Schlegel, Szi-chieh Yu, Claire E. McKellar, Albert Lin, et al. 2024. "Neuronal Wiring Diagram of an Adult Brain." *Nature* 634 (8032): 124–38. https://doi.org/10.1038/s41586-024-07558-y.

Duckhorn, Julia C., Jessica Cande, Mary C. Metkus, Hyeop Song, Sofia Altamirano, David L. Stern, and Troy R. Shirangi. 2022. "Regulation of Drosophila Courtship Behavior by the Tlx/Tailless-like Nuclear Receptor, Dissatisfaction." *Current Biology* 32 (8): 1703-1714.e3. https://doi.org/10.1016/j.cub.2022.02.031.

Enriquez, Jonathan, Lalanti Venkatasubramanian, Myungin Baek, Meredith Peterson, Ulkar Aghayeva, and Richard S. Mann. 2015. "Specification of Individual Adult Motor Neuron Morphologies by Combinatorial Transcription Factor Codes." *Neuron* 86 (4): 955–70. https://doi.org/10.1016/j.neuron.2015.04.011.

Fiddes, Ian T., Gerrald A. Lodewijk, Meghan Mooring, Colleen M. Bosworth, Adam D. Ewing, Gary L. Mantalas, Adam M. Novak, et al. 2018. "Human-Specific NOTCH2NL Genes Affect Notch Signaling and Cortical Neurogenesis." *Cell* 173 (6): 1356-1369.e22. https://doi.org/10.1016/j.cell.2018.03.051.

Finley, K. D., B. J. Taylor, M. Milstein, and M. McKeown. 1997. "Dissatisfaction, a Gene Involved in Sex-Specific Behavior and Neural Development of Drosophila Melanogaster." *Proceedings of the National Academy of Sciences of the United States of America* 94 (3): 913–18. https://doi.org/10.1073/pnas.94.3.913.

Flames, Nuria, Ramón Pla, Diego M. Gelman, John L. R. Rubenstein, Luis Puelles, and Oscar Marín. 2007. "Delineation of Multiple Subpallial Progenitor Domains by the Combinatorial Expression of Transcriptional Codes." *The Journal of Neuroscience* 27 (36): 9682–95. https://doi.org/10.1523/JNEUROSCI.2750-07.2007.

Garnier, Simon, Noam Ross, BoB Rudis, Antoine Filipovic-Pierucci, Tal Galili, Timelyportfolio, Alan O'Callaghan, et al. 2023. "Sjmgarnier/Viridis: CRAN Release v0.6.3." Zenodo. https://doi.org/10.5281/ZENODO.4679423.

Gill, K. S. 1963. "A Mutation Causing Abnormal Courtship and Mating Behavior in Males of Drosophila Melanogaster." 3:507.

Gnerer, Joshua P., Koen J. T. Venken, and Herman A. Dierick. 2015. "Gene-Specific Cell Labeling Using MiMIC Transposons." *Nucleic Acids Research* 43 (8): e56. https://doi.org/10.1093/nar/gkv113.

Goodwin, Stephen F., and Oliver Hobert. 2021. "Molecular Mechanisms of Sexually Dimorphic Nervous System Patterning in Flies and Worms." *Annual Review of Cell and Developmental Biology* 37 (October):519–47. https://doi.org/10.1146/annurev-cellbio-120319-115237.

Hall, Jeffrey C. 1978. "Courtship among Males Due to a Male-Sterile Mutation inDrosophila Melanogaster." *Behavior Genetics* 8 (2): 125–41. https://doi.org/10.1007/BF01066870.

Hao, Yuhan, Tim Stuart, Madeline H. Kowalski, Saket Choudhary, Paul Hoffman, Austin Hartman, Avi Srivastava, et al. 2024. "Dictionary Learning for Integrative, Multimodal and Scalable Single-Cell Analysis." *Nature Biotechnology* 42 (2): 293–304.

https://doi.org/10.1038/s41587-023-01767-y.
Harris, Robin M, Barret D Pfeiffer, Gerald M Rubin, and James W Truman. 2015. "Neuron Hemilineages Provide the Functional Ground Plan for the Drosophila Ventral Nervous System." *eLife* 4 (July):e04493. https://doi.org/10.7554/eLife.04493.
Hay, B.A., T. Wolff, and G.M. Rubin. 1994. "Expression of Baculovirus P35 Prevents Cell Death in Drosophila." *Development* 120 (8): 2121–29. https://doi.org/10.1242/dev.120.8.2121.
Hildebrandt, Kirsten, Christine Klöppel, Jasmin Gogel, Volker Hartenstein, and Uwe Walldorf. 2022. "Orthopedia Expression during Drosophila Melanogaster Nervous System Development and Its Regulation by microRNA-252." *Developmental Biology* 492 (December):87–100. https://doi.org/10.1016/j.ydbio.2022.09.006.
Hobert, Oliver. 2016. "Terminal Selectors of Neuronal Identity." In *Current Topics in Developmental Biology*, 116:455–75. Elsevier. https://doi.org/10.1016/bs.ctdb.2015.12.007.
Holguera, Isabel, and Claude Desplan. 2018. "Neuronal Specification in Space and Time." *Science* 362 (6411): 176–80. https://doi.org/10.1126/science.aas9435.
Hoopfer, Eric D, Yonil Jung, Hidehiko K Inagaki, Gerald M Rubin, and David J Anderson. 2015. "P1 Interneurons Promote a Persistent Internal State That Enhances Inter-Male Aggression in Drosophila." *eLife* 4 (December). https://doi.org/10.7554/elife.11346.
Huang, Da Wei, Brad T Sherman, and Richard A Lempicki. 2009. "Systematic and Integrative Analysis of Large Gene Lists Using DAVID Bioinformatics Resources." *Nature Protocols* 4 (1): 44–57. https://doi.org/10.1038/nprot.2008.211.
Ito, H., K. Fujitani, K. Usui, K. Shimizu-Nishikawa, S. Tanaka, and D. Yamamoto. 1996. "Sexual Orientation in Drosophila Is Altered by the Satori Mutation in the Sex-Determination Gene Fruitless That Encodes a Zinc Finger Protein with a BTB Domain." *Proceedings of the National Academy of Sciences of the United States of America* 93 (18): 9687–92. https://doi.org/10.1073/pnas.93.18.9687.
Ito, Hiroki, Kosei Sato, Shu Kondo, Ryu Ueda, and Daisuke Yamamoto. 2016. "Fruitless Represses Robo1 Transcription to Shape Male-Specific Neural Morphology and Behavior in Drosophila." *Current Biology* 26 (12): 1532–42. https://doi.org/10.1016/j.cub.2016.04.067.
Ito, Masayoshi, Naoki Masuda, Kazunori Shinomiya, Keita Endo, and Kei Ito. 2013. "Systematic Analysis of Neural Projections Reveals Clonal Composition of the Drosophila Brain." *Current Biology* 23 (8): 644–55. https://doi.org/10.1016/j.cub.2013.03.015.
Jain, Saumya, Ying Lin, Yerbol Z. Kurmangaliyev, Javier Valdes-Aleman, Samuel A. LoCascio, Parmis Mirshahidi, Brianna Parrington, and S. Lawrence Zipursky. 2022. "A Global Timing Mechanism Regulates Cell-Type-Specific Wiring Programmes." *Nature* 603 (7899): 112–18. https://doi.org/10.1038/s41586-022-04418-5.
Janssens, Jasper, Sara Aibar, Ibrahim Ihsan Taskiran, Joy N. Ismail, Alicia Estacio Gomez, Gabriel Aughey, Katina I. Spanier, et al. 2022a. "Decoding Gene Regulation in the Fly Brain." *Nature* 601 (7894): 630–36. https://doi.org/10.1038/s41586-021-04262-z.
———. 2022b. "Decoding Gene Regulation in the Fly Brain." *Nature* 601 (7894): 630–36.
Jenett, Arnim, Gerald M. Rubin, Teri-T.B. Ngo, David Shepherd, Christine Murphy, Heather Dionne, Barret D. Pfeiffer, et al. 2012. "A GAL4-Driver Line Resource for Drosophila Neurobiology." *Cell Reports* 2 (4): 991–1001. https://doi.org/10.1016/j.celrep.2012.09.011.

Jessell, Thomas M. 2000. "Neuronal Specification in the Spinal Cord: Inductive Signals and Transcriptional Codes." *Nature Reviews Genetics* 1 (1): 20–29. https://doi.org/10.1038/35049541.

Kallman, Benjamin R, Heesoo Kim, and Kristin Scott. 2015. "Excitation and Inhibition onto Central Courtship Neurons Biases Drosophila Mate Choice." *eLife* 4 (November):e11188. https://doi.org/10.7554/eLife.11188.

Kim, Dong Won, Parris Whitney Washington, Zoe Qianyi Wang, Sonia Hao Lin, Changyu Sun, Basma Taleb Ismail, Hong Wang, Lizhi Jiang, and Seth Blackshaw. 2020. "The Cellular and Molecular Landscape of Hypothalamic Patterning and Differentiation from Embryonic to Late Postnatal Development." *Nature Communications* 11 (1): 4360. https://doi.org/10.1038/s41467-020-18231-z.

Kimura, Ken-ichi, Tomoaki Hachiya, Masayuki Koganezawa, Tatsunori Tazawa, and Daisuke Yamamoto. 2008. "Fruitless and Doublesex Coordinate to Generate Male-Specific Neurons That Can Initiate Courtship." *Neuron* 59 (5): 759–69. https://doi.org/10.1016/j.neuron.2008.06.007.

Kimura, Ken-Ichi, Manabu Ote, Tatsunori Tazawa, and Daisuke Yamamoto. 2005. "Fruitless Specifies Sexually Dimorphic Neural Circuitry in the Drosophila Brain." *Nature* 438 (7065): 229–33. https://doi.org/10.1038/nature04229.

Koganezawa, Masayuki, Daisuke Haba, Takashi Matsuo, and Daisuke Yamamoto. 2010. "The Shaping of Male Courtship Posture by Lateralized Gustatory Inputs to Male-Specific Interneurons." *Current Biology* 20 (1): 1–8. https://doi.org/10.1016/j.cub.2009.11.038.

Koganezawa, Masayuki, Ken-Ichi Kimura, and Daisuke Yamamoto. 2016. "The Neural Circuitry That Functions as a Switch for Courtship versus Aggression in Drosophila Males." *Current Biology: CB* 26 (11): 1395–1403. https://doi.org/10.1016/j.cub.2016.04.017.

Kohl, Johannes, Aaron D. Ostrovsky, Shahar Frechter, and Gregory S. X. E. Jefferis. 2013. "A Bidirectional Circuit Switch Reroutes Pheromone Signals in Male and Female Brains." *Cell* 155 (7): 1610–23. https://doi.org/10.1016/j.cell.2013.11.025.

Kohwi, Minoree, and Chris Q. Doe. 2013. "Temporal Fate Specification and Neural Progenitor Competence during Development." *Nature Reviews Neuroscience* 14 (12): 823–38. https://doi.org/10.1038/nrn3618.

Kohwi, Minoree, Laurel S. Hiebert, and Chris Q. Doe. 2011. "The Pipsqueak-Domain Proteins Distal Antenna and Distal Antenna-Related Restrict Hunchback Neuroblast Expression and Early-Born Neuronal Identity." *Development* 138 (9): 1727–35. https://doi.org/10.1242/dev.061499.

Konstantinides, Nikolaos, Isabel Holguera, Anthony M. Rossi, Aristides Escobar, Liébaut Dudragne, Yen-Chung Chen, Thinh N. Tran, et al. 2022. "A Complete Temporal Transcription Factor Series in the Fly Visual System." *Nature* 604 (7905): 316–22. https://doi.org/10.1038/s41586-022-04564-w.

Konstantinides, Nikolaos, Katarina Kapuralin, Chaimaa Fadil, Luendreo Barboza, Rahul Satija, and Claude Desplan. 2018. "Phenotypic Convergence: Distinct Transcription Factors Regulate Common Terminal Features." *Cell* 174 (3): 622-635.e13. https://doi.org/10.1016/j.cell.2018.05.021.

Kurusu, Mitsuhiko, Tomoko Nagao, Uwe Walldorf, Susanne Flister, Walter J. Gehring, and Katsuo Furukubo-Tokunaga. 2000. "Genetic Control of Development of the Mushroom Bodies, the Associative Learning Centers in the *Drosophila* Brain, by the *Eyeless, Twin of Eyeless* , and *Dachshund* Genes." *Proceedings of the National Academy of Sciences* 97

(5): 2140–44. https://doi.org/10.1073/pnas.040564497.
Lacin, Haluk, Hui-Min Chen, Xi Long, Robert H Singer, Tzumin Lee, and James W Truman. 2019. "Neurotransmitter Identity Is Acquired in a Lineage-Restricted Manner in the Drosophila CNS." *eLife* 8 (March):e43701. https://doi.org/10.7554/eLife.43701.
Lacin, Haluk, Jannette Rusch, Raymond T. Yeh, Miki Fujioka, Beth A. Wilson, Yi Zhu, Alice A. Robie, et al. 2014. "Genome-Wide Identification of Drosophila Hb9 Targets Reveals a Pivotal Role in Directing the Transcriptome within Eight Neuronal Lineages, Including Activation of Nitric Oxide Synthase and Fd59a/Fox-D." *Developmental Biology* 388 (1): 117–33. https://doi.org/10.1016/j.ydbio.2014.01.029.
Lacin, Haluk, W Ryan Williamson, Gwyneth M Card, James B Skeath, and James W Truman. 2020. "Unc-4 Acts to Promote Neuronal Identity and Development of the Take-off Circuit in the Drosophila CNS." *eLife* 9 (March):e55007. https://doi.org/10.7554/eLife.55007.
Lacin, Haluk, Yi Zhu, Beth A. Wilson, and James B. Skeath. 2014. "Transcription Factor Expression Uniquely Identifies Most Postembryonic Neuronal Lineages in the *Drosophila* Thoracic Central Nervous System." *Development* 141 (5): 1011–21. https://doi.org/10.1242/dev.102178.
Larsen, Camilla, Diana Shy, Shana R. Spindler, Siaumin Fung, Wayne Pereanu, Amelia Younossi-Hartenstein, and Volker Hartenstein. 2009. "Patterns of Growth, Axonal Extension and Axonal Arborization of Neuronal Lineages in the Developing Drosophila Brain." *Developmental Biology* 335 (2): 289–304. https://doi.org/10.1016/j.ydbio.2009.06.015.
Lee, T., and L. Luo. 1999. "Mosaic Analysis with a Repressible Cell Marker for Studies of Gene Function in Neuronal Morphogenesis." *Neuron* 22 (3): 451–61. https://doi.org/10.1016/s0896-6273(00)80701-1.
Lee, Ying-Jou, Ching-Po Yang, Rosa L Miyares, Yu-Fen Huang, Yisheng He, Qingzhong Ren, Hui-Min Chen, et al. 2020. "Conservation and Divergence of Related Neuronal Lineages in the Drosophila Central Brain." *eLife* 9 (April):e53518. https://doi.org/10.7554/eLife.53518.
Lenschow, Constanze, and Susana Q Lima. 2020. "In the Mood for Sex: Neural Circuits for Reproduction." *Current Opinion in Neurobiology* 60 (February):155–68. https://doi.org/10.1016/j.conb.2019.12.001.
Li, Hongjie, Felix Horns, Bing Wu, Qijing Xie, Jiefu Li, Tongchao Li, David J. Luginbuhl, Stephen R. Quake, and Liqun Luo. 2017. "Classifying Drosophila Olfactory Projection Neuron Subtypes by Single-Cell RNA Sequencing." *Cell* 171 (5): 1206-1220.e22. https://doi.org/10.1016/j.cell.2017.10.019.
Lichtneckert, Robert, and Heinrich Reichert. 2008. "Anteroposterior Regionalization of the Brain: Genetic and Comparative Aspects." In *Brain Development in Drosophila Melanogaster*, edited by Gerhard M. Technau, 628:32–41. Advances in Experimental Medicine and Biology. New York, NY: Springer New York. https://doi.org/10.1007/978-0-387-78261-4_2.
Lillvis, Joshua L., Kaiyu Wang, Hiroshi M. Shiozaki, Min Xu, David L. Stern, and Barry J. Dickson. 2024. "Nested Neural Circuits Generate Distinct Acoustic Signals during Drosophila Courtship." *Current Biology* 34 (4): 808-824.e6. https://doi.org/10.1016/j.cub.2024.01.015.
Lin, Suewei, Chih-Fei Kao, Hung-Hsiang Yu, Yaling Huang, and Tzumin Lee. 2012. "Lineage

Analysis of Drosophila Lateral Antennal Lobe Neurons Reveals Notch-Dependent Binary Temporal Fate Decisions." *PLoS Biology* 10 (11): e1001425. https://doi.org/10.1371/journal.pbio.1001425.

Lin, Suewei, Sen-Lin Lai, Huang-Hsiang Yu, Takahiro Chihara, Liqun Luo, and Tzumin Lee. 2010. "Lineage-Specific Effects of Notch/Numb Signaling in Post-Embryonic Development of the *Drosophila* Brain." *Development* 137 (1): 43–51. https://doi.org/10.1242/dev.041699.

Liu, Ling-Yu, Xi Long, Ching-Po Yang, Rosa L Miyares, Ken Sugino, Robert H Singer, and Tzumin Lee. 2019. "Mamo Decodes Hierarchical Temporal Gradients into Terminal Neuronal Fate." *eLife* 8 (September):e48056. https://doi.org/10.7554/eLife.48056.

Liu, Zhiyong, Ching-Po Yang, Ken Sugino, Chi-Cheng Fu, Ling-Yu Liu, Xiaohao Yao, Luke P. Lee, and Tzumin Lee. 2015. "Opposing Intrinsic Temporal Gradients Guide Neural Stem Cell Production of Varied Neuronal Fates." *Science* 350 (6258): 317–20. https://doi.org/10.1126/science.aad1886.

Lovick, Jennifer K., Kathy T. Ngo, Jaison J. Omoto, Darren C. Wong, Joseph D. Nguyen, and Volker Hartenstein. 2013. "Postembryonic Lineages of the Drosophila Brain: I. Development of the Lineage-Associated Fiber Tracts." *Developmental Biology* 384 (2): 228–57. https://doi.org/10.1016/j.ydbio.2013.07.008.

Lyu, Pin, Thanh Hoang, Clayton P. Santiago, Eric D. Thomas, Andrew E. Timms, Haley Appel, Megan Gimmen, et al. 2021a. "Gene Regulatory Networks Controlling Temporal Patterning, Neurogenesis, and Cell-Fate Specification in Mammalian Retina." *Cell Reports* 37 (7): 109994. https://doi.org/10.1016/j.celrep.2021.109994.

———. 2021b. "Gene Regulatory Networks Controlling Temporal Patterning, Neurogenesis, and Cell-Fate Specification in Mammalian Retina." *Cell Reports* 37 (7): 109994. https://doi.org/10.1016/j.celrep.2021.109994.

Mance, Lucija, Nicolas Bigot, Edison Zhamungui Sánchez, Franck Coste, Natalia Martín-González, Siham Zentout, Marin Biliškov, et al. 2024. "Dynamic BTB-Domain Filaments Promote Clustering of ZBTB Proteins." *Molecular Cell* 84 (13): 2490-2510.e9. https://doi.org/10.1016/j.molcel.2024.05.029.

Manoli, Devanand S., and Bruce S. Baker. 2004. "Median Bundle Neurons Coordinate Behaviours during Drosophila Male Courtship." *Nature* 430 (6999): 564–69. https://doi.org/10.1038/nature02713.

Manoli, Devanand S., Margit Foss, Adriana Villella, Barbara J. Taylor, Jeffrey C. Hall, and Bruce S. Baker. 2005. "Male-Specific Fruitless Specifies the Neural Substrates of Drosophila Courtship Behaviour." *Nature* 436 (7049): 395–400. https://doi.org/10.1038/nature03859.

Mark, Brandon, Sen-Lin Lai, Aref Arzan Zarin, Laurina Manning, Heather Q Pollington, Ashok Litwin-Kumar, Albert Cardona, James W Truman, and Chris Q Doe. 2021. "A Developmental Framework Linking Neurogenesis and Circuit Formation in the Drosophila CNS." *eLife* 10 (May):e67510. https://doi.org/10.7554/eLife.67510.

Maurange, Cédric, Louise Cheng, and Alex P. Gould. 2008. "Temporal Transcription Factors and Their Targets Schedule the End of Neural Proliferation in Drosophila." *Cell* 133 (5): 891–902. https://doi.org/10.1016/j.cell.2008.03.034.

Mellert, David J., Jon-Michael Knapp, Devanand S. Manoli, Geoffrey W. Meissner, and Bruce S. Baker. 2010. "Midline Crossing by Gustatory Receptor Neuron Axons Is Regulated by Fruitless, Doublesex and the Roundabout Receptors." *Development (Cambridge,*

England) 137 (2): 323–32. https://doi.org/10.1242/dev.045047.
Minocha, Shilpi, Werner Boll, and Markus Noll. 2017. "Crucial Roles of Pox Neuro in the Developing Ellipsoid Body and Antennal Lobes of the Drosophila Brain." Edited by Efthimios M. C. Skoulakis. *PLOS ONE* 12 (4): e0176002. https://doi.org/10.1371/journal.pone.0176002.
Miyares, Rosa Linda, and Tzumin Lee. 2019. "Temporal Control of Drosophila Central Nervous System Development." *Current Opinion in Neurobiology* 56 (June):24–32. https://doi.org/10.1016/j.conb.2018.10.016.
Muhr, Jonas, Elisabet Andersson, Madelen Persson, Thomas M. Jessell, and Johan Ericson. 2001. "Groucho-Mediated Transcriptional Repression Establishes Progenitor Cell Pattern and Neuronal Fate in the Ventral Neural Tube." *Cell* 104 (6): 861–73. https://doi.org/10.1016/S0092-8674(01)00283-5.
Nagarkar-Jaiswal, Sonal, Pei-Tseng Lee, Megan E Campbell, Kuchuan Chen, Stephanie Anguiano-Zarate, Manuel Cantu Gutierrez, Theodore Busby, et al. 2015. "A Library of MiMICs Allows Tagging of Genes and Reversible, Spatial and Temporal Knockdown of Proteins in Drosophila." *eLife* 4 (March):e05338. https://doi.org/10.7554/eLife.05338.
Neuwirth, Erich. 2022. "RColorBrewer: ColorBrewer Palettes." https://doi.org/10.32614/CRAN.package.RColorBrewer.
Noveen, Alexander, Ann Daniel, and Volker Hartenstein. 2000. "Early Development of the *Drosophila* Mushroom Body: The Roles of *Eyeless* and *Dachshund*." *Development* 127 (16): 3475–88. https://doi.org/10.1242/dev.127.16.3475.
Oren-Suissa, Meital, and Troy R. Shirangi. 2025. "Neural Circuits Underlying Sexually Dimorphic Innate Behaviors." *Annual Review of Neuroscience*, March. https://doi.org/10.1146/annurev-neuro-112723-034621.
Özel, Mehmet Neset, Claudia Skok Gibbs, Isabel Holguera, Mennah Soliman, Richard Bonneau, and Claude Desplan. 2022. "Coordinated Control of Neuronal Differentiation and Wiring by Sustained Transcription Factors." *Science* 378 (6626): eadd1884. https://doi.org/10.1126/science.add1884.
Park, Paul M.C., Jiho Park, Jared Brown, Moritz Hunkeler, Shourya S. Roy Burman, Katherine A. Donovan, Hojong Yoon, et al. 2024. "Polymerization of ZBTB Transcription Factors Regulates Chromatin Occupancy." *Molecular Cell* 84 (13): 2511-2524.e8. https://doi.org/10.1016/j.molcel.2024.06.010.
Pereanu, Wayne, and Volker Hartenstein. 2006. "Neural Lineages of the*Drosophila*Brain: A Three-Dimensional Digital Atlas of the Pattern of Lineage Location and Projection at the Late Larval Stage." *The Journal of Neuroscience* 26 (20): 5534–53. https://doi.org/10.1523/jneurosci.4708-05.2006.
Pfeiffer, Barret D., James W. Truman, and Gerald M. Rubin. 2012. "Using Translational Enhancers to Increase Transgene Expression in *Drosophila*." *Proceedings of the National Academy of Sciences* 109 (17): 6626–31. https://doi.org/10.1073/pnas.1204520109.
Pignoni, Francesca, and S. Lawrence Zipursky. 1997. "Induction of *Drosophila* Eye Development by Decapentaplegic." *Development* 124 (2): 271–78. https://doi.org/10.1242/dev.124.2.271.
Reilly, Molly B., Cyril Cros, Erdem Varol, Eviatar Yemini, and Oliver Hobert. 2020. "Unique Homeobox Codes Delineate All the Neuron Classes of C. Elegans." *Nature* 584 (7822): 595–601. https://doi.org/10.1038/s41586-020-2618-9.
Ren, Qingzhong, Takeshi Awasaki, Yu-Fen Huang, Zhiyong Liu, and Tzumin Lee. 2016. "Cell

Class-Lineage Analysis Reveals Sexually Dimorphic Lineage Compositions in the Drosophila Brain." *Current Biology* 26 (19): 2583–93. https://doi.org/10.1016/j.cub.2016.07.086.

Ren, Xingjie, Jin Sun, Benjamin E. Housden, Yanhui Hu, Charles Roesel, Shuailiang Lin, Lu-Ping Liu, et al. 2013. "Optimized Gene Editing Technology for *Drosophila Melanogaster* Using Germ Line-Specific Cas9." *Proceedings of the National Academy of Sciences* 110 (47): 19012–17. https://doi.org/10.1073/pnas.1318481110.

Roggenbuck, Emma C., Elijah A. Hall, Isabel B. Hanson, Alyssa A. Roby, Katherine K. Zhang, Kyle A. Alkatib, Joseph A. Carter, et al. 2024. "Let's Talk about Sex: Mechanisms of Neural Sexual Differentiation in Bilateria." *WIREs Mechanisms of Disease* 16 (2): e1636. https://doi.org/10.1002/wsbm.1636.

Roome, Robert Brian, Archana Yadav, Lydia Flores, Amrit Puarr, Diana Nardini, Alexander Richardson, Ronald R. Waclaw, et al. 2025. "Ontogeny of the Spinal Cord Dorsal Horn." Neuroscience. https://doi.org/10.1101/2025.03.14.643370.

Rossi, Anthony M, and Claude Desplan. 2020. "Extrinsic Activin Signaling Cooperates with an Intrinsic Temporal Program to Increase Mushroom Body Neuronal Diversity." *eLife* 9 (July):e58880. https://doi.org/10.7554/eLife.58880.

Ruta, Vanessa, Sandeep Robert Datta, Maria Luisa Vasconcelos, Jessica Freeland, Loren L. Looger, and Richard Axel. 2010. "A Dimorphic Pheromone Circuit in Drosophila from Sensory Input to Descending Output." *Nature* 468 (7324): 686–90. https://doi.org/10.1038/nature09554.

Ryner, L. C., S. F. Goodwin, D. H. Castrillon, A. Anand, A. Villella, B. S. Baker, J. C. Hall, B. J. Taylor, and S. A. Wasserman. 1996. "Control of Male Sexual Behavior and Sexual Orientation in Drosophila by the Fruitless Gene." *Cell* 87 (6): 1079–89. https://doi.org/10.1016/s0092-8674(00)81802-4.

Sagner, Andreas, and James Briscoe. 2019. "Establishing Neuronal Diversity in the Spinal Cord: A Time and a Place." *Development* 146 (22): dev182154. https://doi.org/10.1242/dev.182154.

Samuel Marsh, Maëlle Salmon, Paul Hoffman, and kew24. 2024. "Samuel-Marsh/scCustomize: Version 3.0.1." Zenodo. https://doi.org/10.5281/ZENODO.5706430.

Schindelin, Johannes, Ignacio Arganda-Carreras, Erwin Frise, Verena Kaynig, Mark Longair, Tobias Pietzsch, Stephan Preibisch, et al. 2012. "Fiji: An Open-Source Platform for Biological-Image Analysis." *Nature Methods* 9 (7): 676–82. https://doi.org/10.1038/nmeth.2019.

Schlegel, Philipp, Yijie Yin, Alexander S. Bates, Sven Dorkenwald, Katharina Eichler, Paul Brooks, Daniel S. Han, et al. 2024. "Whole-Brain Annotation and Multi-Connectome Cell Typing of Drosophila." *Nature* 634 (8032): 139–52. https://doi.org/10.1038/s41586-024-07686-5.

Schwarzkopf, Maayan, Mike C. Liu, Samuel J. Schulte, Rachel Ives, Naeem Husain, Harry M. T. Choi, and Niles A. Pierce. 2021. "Hybridization Chain Reaction Enables a Unified Approach to Multiplexed, Quantitative, High-Resolution Immunohistochemistry and *in Situ* Hybridization." *Development* 148 (22): dev199847. https://doi.org/10.1242/dev.199847.

Sen, Sonia Q. 2023. "Generating Neural Diversity through Spatial and Temporal Patterning." *Seminars in Cell & Developmental Biology* 142 (June):54–66. https://doi.org/10.1016/j.semcdb.2022.06.002.

Sen, Sonia Q, Sachin Chanchani, Tony D Southall, and Chris Q Doe. 2019. "Neuroblast-Specific Open Chromatin Allows the Temporal Transcription Factor, Hunchback, to Bind Neuroblast-Specific Loci." *eLife* 8 (January):e44036. https://doi.org/10.7554/eLife.44036.

Sengupta, Saheli, Yick-Bun Chan, Caroline B. Palavicino-Maggio, and Edward A. Kravitz. 2022. "GABA Transmission from mAL Interneurons Regulates Aggression in *Drosophila* Males." *Proceedings of the National Academy of Sciences* 119 (5): e2117101119. https://doi.org/10.1073/pnas.2117101119.

Serrano-Saiz, Esther, Burcu Gulez, Laura Pereira, Marie Gendrel, Sze Yen Kerk, Berta Vidal, Weidong Feng, et al. 2020. "Modular Organization of *Cis* -Regulatory Control Information of Neurotransmitter Pathway Genes in *Caenorhabditis Elegans*." *Genetics* 215 (3): 665–81. https://doi.org/10.1534/genetics.120.303206.

Sherman, Brad T, Ming Hao, Ju Qiu, Xiaoli Jiao, Michael W Baseler, H Clifford Lane, Tomozumi Imamichi, and Weizhong Chang. 2022. "DAVID: A Web Server for Functional Enrichment Analysis and Functional Annotation of Gene Lists (2021 Update)." *Nucleic Acids Research* 50 (W1): W216–21. https://doi.org/10.1093/nar/gkac194.

Simon, Félix, Isabel Holguera, Yen-Chung Chen, Jennifer Malin, Priscilla Valentino, Claire Njoo-Deplante, Rana Naja El-Danaf, et al. 2025. "Establishment of Terminal Selector Combinations in Optic Lobe Neurons." *bioRxiv: The Preprint Server for Biology*, January, 2024.02.05.578975. https://doi.org/10.1101/2024.02.05.578975.

Smolin, Natalie, Mark Dombrovski, Bryce W. Hina, Anthony Moreno-Sanchez, Ryan Gossart, Catherine R. Carmona, Aadil Rehan, et al. 2024. "Neuronal Identity Control at the Resolution of a Single Transcription Factor Isoform." *bioRxiv: The Preprint Server for Biology*, June, 2024.06.14.598883. https://doi.org/10.1101/2024.06.14.598883.

Snell, Nathaniel J., John D. Fisher, Griffin G. Hartmann, Bence Zolyomi, Mustafa Talay, and Gilad Barnea. 2022. "Complex Representation of Taste Quality by Second-Order Gustatory Neurons in Drosophila." *Current Biology* 32 (17): 3758-3772.e4. https://doi.org/10.1016/j.cub.2022.07.048.

Soffers, Jelly Hm, Erin Beck, Daniel J Sytkowski, Marianne E Maughan, Devasri Devarakonda, Yi Zhu, Beth Wilson, et al. 2025. "A Library of Lineage-Specific Driver Lines Connects Developing Neuronal Circuits to Behavior in the Drosophila Ventral Nerve Cord." eLife Sciences Publications, Ltd. https://doi.org/10.7554/elife.106042.2.

Spana, E. P., and C. Q. Doe. 1996. "Numb Antagonizes Notch Signaling to Specify Sibling Neuron Cell Fates." *Neuron* 17 (1): 21–26. https://doi.org/10.1016/s0896-6273(00)80277-9.

Spindler, Shana R., and Volker Hartenstein. 2010. "The Drosophila Neural Lineages: A Model System to Study Brain Development and Circuitry." *Development Genes and Evolution* 220 (1–2): 1–10. https://doi.org/10.1007/s00427-010-0323-7.

Stockinger, Petra, Duda Kvitsiani, Shay Rotkopf, László Tirián, and Barry J. Dickson. 2005. "Neural Circuitry That Governs Drosophila Male Courtship Behavior." *Cell* 121 (5): 795–807. https://doi.org/10.1016/j.cell.2005.04.026.

Sweeney, Lora B., Jay B. Bikoff, Mariano I. Gabitto, Susan Brenner-Morton, Myungin Baek, Jerry H. Yang, Esteban G. Tabak, Jeremy S. Dasen, Christopher R. Kintner, and Thomas M. Jessell. 2018. "Origin and Segmental Diversity of Spinal Inhibitory Interneurons." *Neuron* 97 (2): 341-355.e3. https://doi.org/10.1016/j.neuron.2017.12.029.

Syed, Mubarak Hussain, Brandon Mark, and Chris Q Doe. 2017. "Steroid Hormone Induction of Temporal Gene Expression in Drosophila Brain Neuroblasts Generates Neuronal and Glial Diversity." *eLife* 6 (April):e26287. https://doi.org/10.7554/eLife.26287.

Tang, Jocelyn L.Y., Anna E. Hakes, Robert Krautz, Takumi Suzuki, Esteban G. Contreras, Paul M. Fox, and Andrea H. Brand. 2022. "NanoDam Identifies Homeobrain (ARX) and Scarecrow (NKX2.1) as Conserved Temporal Factors in the Drosophila Central Brain and Visual System." *Developmental Cell* 57 (9): 1193-1207.e7. https://doi.org/10.1016/j.devcel.2022.04.008.

Thomas, John B., Michael J. Bastiani, Michael Bate, and Corey S. Goodman. 1984. "From Grasshopper to Drosophila: A Common Plan for Neuronal Development." *Nature* 310 (5974): 203–7. https://doi.org/10.1038/310203a0.

Truman, J. W., and Eldon E. Ball. 1998. "Patterns of Embryonic Neurogenesis in a Primitive Wingless Insect, the Silverfish, Ctenolepisma Longicaudata: Comparison with Those Seen in Flying Insects." *Development Genes and Evolution* 208 (7): 357–68. https://doi.org/10.1007/s004270050192.

Truman, James W., and Michael Bate. 1988. "Spatial and Temporal Patterns of Neurogenesis in the Central Nervous System of Drosophila Melanogaster." *Developmental Biology* 125 (1): 145–57. https://doi.org/10.1016/0012-1606(88)90067-X.

Truman, James W., Wanda Moats, Janet Altman, Elizabeth C. Marin, and Darren W. Williams. 2010. "Role of Notch Signaling in Establishing the Hemilineages of Secondary Neurons in *Drosophila Melanogaster*." *Development* 137 (1): 53–61. https://doi.org/10.1242/dev.041749.

Urbach, Rolf, David Jussen, and Gerhard M. Technau. 2016. "Gene Expression Profiles Uncover Individual Identities of Gnathal Neuroblasts and Serial Homologies in the Embryonic CNS of *Drosophila*." *Development* 143 (8): 1290–1301. https://doi.org/10.1242/dev.133546.

Urbach, Rolf, Ralf Schnabel, and Gerhard M. Technau. 2003. "The Pattern of Neuroblast Formation, Mitotic Domains and Proneural Gene Expression during Early Brain Development in *Drosophila*." *Development* 130 (16): 3589–3606. https://doi.org/10.1242/dev.00528.

Urbach, Rolf, and Gerhard M. Technau. 2004. "Neuroblast Formation and Patterning during Early Brain Development in *Drosophila*." *BioEssays* 26 (7): 739–51. https://doi.org/10.1002/bies.20062.

———. 2008. "Dorsoventral Patterning of the Brain: A Comparative Approach." In *Brain Development in Drosophila Melanogaster*, edited by Gerhard M. Technau, 628:42–56. Advances in Experimental Medicine and Biology. New York, NY: Springer New York. https://doi.org/10.1007/978-0-387-78261-4_3.

Venken, Koen J T, Karen L Schulze, Nele A Haelterman, Hongling Pan, Yuchun He, Martha Evans-Holm, Joseph W Carlson, et al. 2011. "MiMIC: A Highly Versatile Transposon Insertion Resource for Engineering Drosophila Melanogaster Genes." *Nature Methods* 8 (9): 737–43. https://doi.org/10.1038/nmeth.1662.

von Philipsborn, Anne C., Sabrina Jörchel, Laszlo Tirian, Ebru Demir, Tomoko Morita, David L. Stern, and Barry J. Dickson. 2014. "Cellular and Behavioral Functions of Fruitless Isoforms in Drosophila Courtship." *Current Biology* 24 (3): 242–51. https://doi.org/10.1016/j.cub.2013.12.015.

Waddington, C. H. 1957. *The Strategy of the Genes.* London: George Allen & Unwin.

Wang, Fei, Kaiyu Wang, Nora Forknall, Christopher Patrick, Tansy Yang, Ruchi Parekh, Davi Bock, and Barry J. Dickson. 2020. "Neural Circuitry Linking Mating and Egg Laying in Drosophila Females." *Nature* 579 (7797): 101–5. https://doi.org/10.1038/s41586-020-2055-9.

Wang, Kaiyu, Fei Wang, Nora Forknall, Tansy Yang, Christopher Patrick, Ruchi Parekh, and Barry J. Dickson. 2021. "Neural Circuit Mechanisms of Sexual Receptivity in Drosophila Females." *Nature* 589 (7843): 577–81. https://doi.org/10.1038/s41586-020-2972-7.

West, Emma R., Sylvain W. Lapan, ChangHee Lee, Kathrin M. Kajderowicz, Xihao Li, and Constance L. Cepko. 2022. "Spatiotemporal Patterns of Neuronal Subtype Genesis Suggest Hierarchical Development of Retinal Diversity." *Cell Reports* 38 (1): 110191. https://doi.org/10.1016/j.celrep.2021.110191.

Wickham, Hadley, Mara Averick, Jennifer Bryan, Winston Chang, Lucy McGowan, Romain François, Garrett Grolemund, et al. 2019. "Welcome to the Tidyverse." *Journal of Open Source Software* 4 (43): 1686. https://doi.org/10.21105/joss.01686.

Wong, Darren C., Jennifer K. Lovick, Kathy T. Ngo, Wichanee Borisuthirattana, Jaison J. Omoto, and Volker Hartenstein. 2013. "Postembryonic Lineages of the Drosophila Brain: II. Identification of Lineage Projection Patterns Based on MARCM Clones." *Developmental Biology* 384 (2): 258–89. https://doi.org/10.1016/j.ydbio.2013.07.009.

Xiao, Yangbo, Ye Yuan, and Swathi Yadlapalli. 2022. "A One-Step CRISPR-Based Strategy for Endogenous Gene Tagging in Drosophila Melanogaster." Cold Spring Harbor Laboratory. https://doi.org/10.1101/2022.04.04.487042.

Xu, Chundi, Tyler B. Ramos, Edward M. Rogers, Michael B. Reiser, and Chris Q. Doe. 2023. "Homeodomain Proteins Hierarchically Specify Neuronal Diversity and Synaptic Connectivity." https://doi.org/10.7554/eLife.90133.2.

Yamamoto, Daisuke, and Masayuki Koganezawa. 2013. "Genes and Circuits of Courtship Behaviour in Drosophila Males." *Nature Reviews Neuroscience* 14 (10): 681–92. https://doi.org/10.1038/nrn3567.

Yao, Zizhen, Cindy T. J. Van Velthoven, Michael Kunst, Meng Zhang, Delissa McMillen, Changkyu Lee, Won Jung, et al. 2023. "A High-Resolution Transcriptomic and Spatial Atlas of Cell Types in the Whole Mouse Brain." *Nature* 624 (7991): 317–32. https://doi.org/10.1038/s41586-023-06812-z.

Yapici, Nilay, Manuel Zimmer, and Ana I Domingos. 2014. "Cellular and Molecular Basis of Decision-making." *EMBO Reports* 15 (10): 1023–35. https://doi.org/10.15252/embr.201438993.

Yu, Hung-Hsiang, Takeshi Awasaki, Mark David Schroeder, Fuhui Long, Jacob S. Yang, Yisheng He, Peng Ding, et al. 2013. "Clonal Development and Organization of the Adult Drosophila Central Brain." *Current Biology* 23 (8): 633–43. https://doi.org/10.1016/j.cub.2013.02.057.

Yu, Hung-Hsiang, Chih-Fei Kao, Yisheng He, Peng Ding, Jui-Chun Kao, and Tzumin Lee. 2010. "A Complete Developmental Sequence of a Drosophila Neuronal Lineage as Revealed by Twin-Spot MARCM." Edited by Hugo J. Bellen. *PLoS Biology* 8 (8): e1000461. https://doi.org/10.1371/journal.pbio.1000461.

Yu, Jai Y., Makoto I. Kanai, Ebru Demir, Gregory S.X.E. Jefferis, and Barry J. Dickson. 2010. "Cellular Organization of the Neural Circuit That Drives Drosophila Courtship Behavior." *Current Biology* 20 (18): 1602–14. https://doi.org/10.1016/j.cub.2010.08.025.

Zappia, Luke, and Alicia Oshlack. 2018. "Clustering Trees: A Visualization for Evaluating

Clusterings at Multiple Resolutions." *GigaScience* 7 (7): giy083. https://doi.org/10.1093/gigascience/giy083.

Zhang, Stephen X., Lauren E. Miner, Christine L. Boutros, Dragana Rogulja, and Michael A. Crickmore. 2018. "Motivation, Perception, and Chance Converge to Make a Binary Decision." *Neuron* 99 (2): 376-388.e6. https://doi.org/10.1016/j.neuron.2018.06.014.

Zheng, Zhihao, J. Scott Lauritzen, Eric Perlman, Camenzind G. Robinson, Matthew Nichols, Daniel Milkie, Omar Torrens, et al. 2018. "A Complete Electron Microscopy Volume of the Brain of Adult Drosophila Melanogaster." *Cell* 174 (3): 730-743.e22. https://doi.org/10.1016/j.cell.2018.06.019.

Zhu, Sijun, Suewei Lin, Chih-Fei Kao, Takeshi Awasaki, Ann-Shyn Chiang, and Tzumin Lee. 2006. "Gradients of the Drosophila Chinmo BTB-Zinc Finger Protein Govern Neuronal Temporal Identity." *Cell* 127 (2): 409–22. https://doi.org/10.1016/j.cell.2006.08.045.

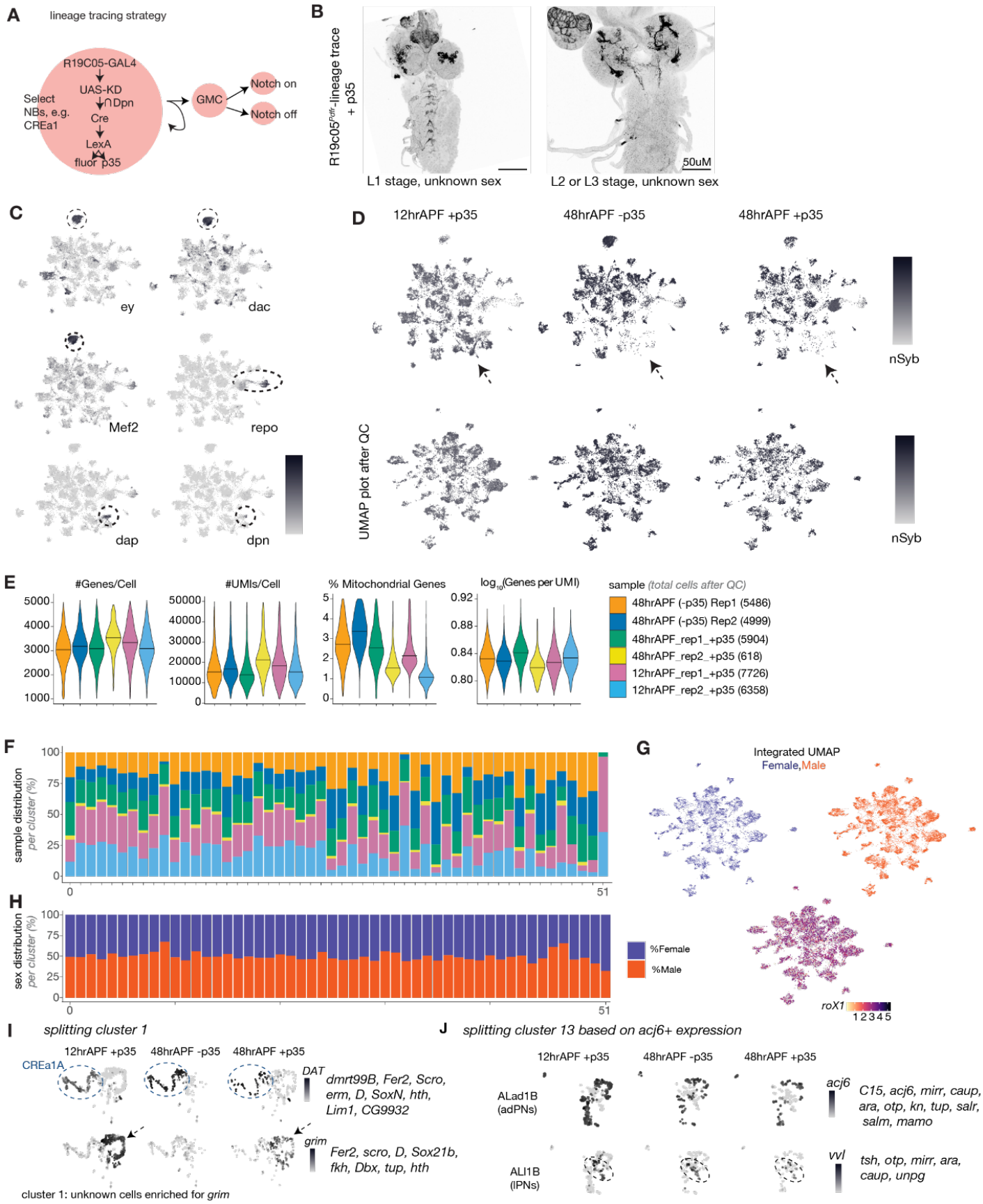

Figure S1: Data related to Figure 1

A. The R19C05 fragment of *pdfr* drives expression of GAL4 in CREa1 and other neuroblasts (Q. Ren et al. 2016). GAL4 drives KD recombinase. The intersection of KD and the neuroblast-specific deadpan promoter activates Cre.

Cre excises a stop codon upstream of LexA. This results in permanent LexA expression in the NB and its daughters, which can be used to drive expression of effectors. Genetic strategy adapted from (Awasaki et al. 2014). B. R19C05 Clonal labeling strategy in early larval stages (L1) vs L2/L3 determined by mouth hooks. C. UMAP feature plots of pre-filtered scRNA-seq data from R19C05-labelled lineages. *Ey*, *dac* and *Mef2* mark Kenyon cells, *repo* marks glia and *dpn* and *dap* mark progenitor cells. D. UMAP feature plots of nSyb expression split across timepoints (12hrAPF and 48hrAPF) and conditions (+/-p35) before filtering *nSyb* low cells (top) and after (bottom). E. The number of genes, UMIs, percent mitochondrial gene expression and the "library complexity" (log10 genes/log10 UMI) across cells for each library after filtering. The final number of cells from each dataset is between parentheses. F. The proportion of cells coming from each of our 6 datasets for every cluster. G. Sexing cells using *lncRNA:roX1* and *lnRNA:roX2* and contribution of male and females cells across the integrated UMAP. H. The proportion of cells coming from males versus females based on the expression of *lncRNA:roX1* and *lnRNA:roX2*. I. Basis and method for splitting clusters 1 and 13 into distinct hemilineage clusters.

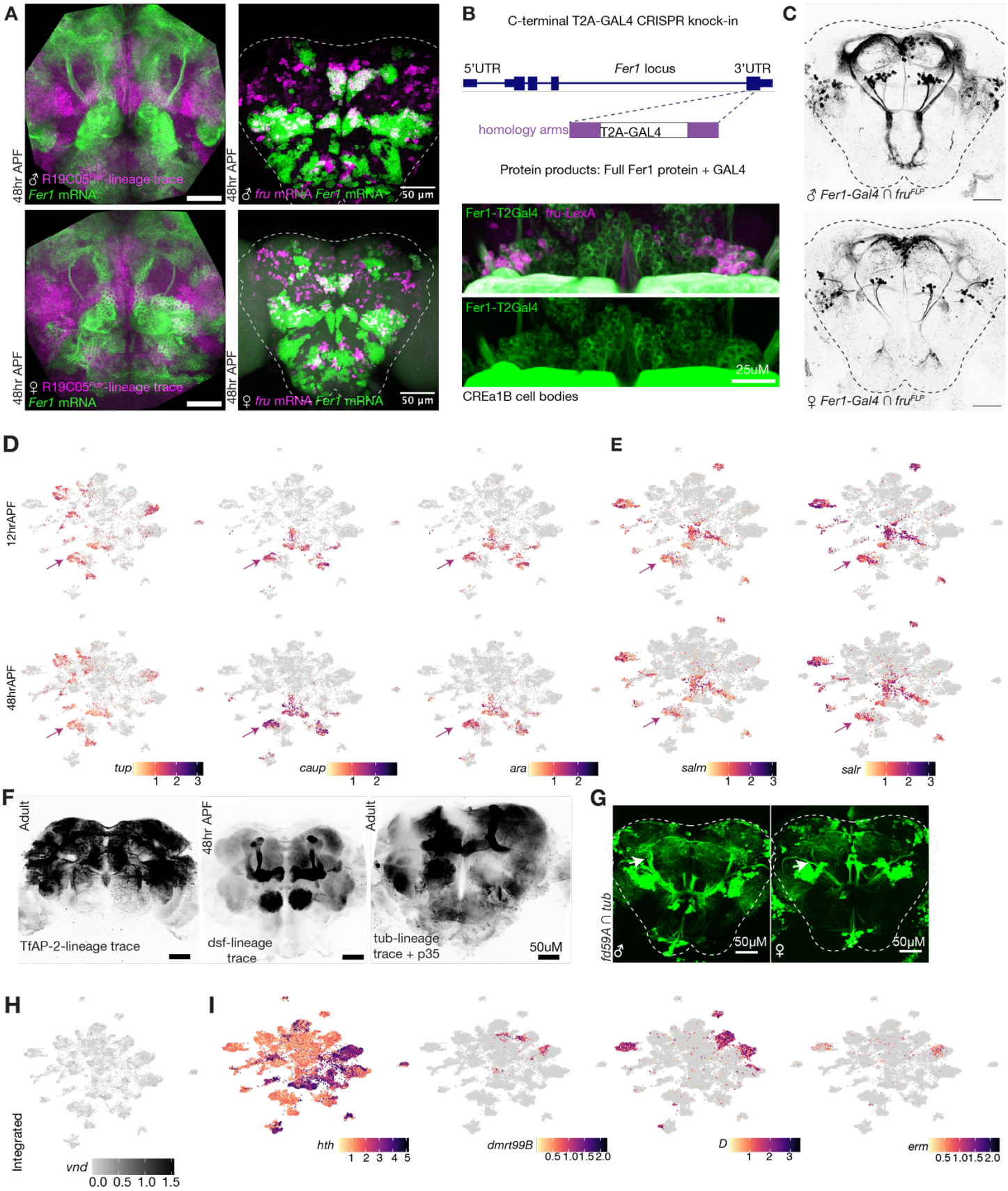

Figure S2: Data related to Figure 2

A. (Left) R19C05 Clonal labeling strategy combined with RNA FISH for *Fer1* at 48hrAPF. (Right) RNA FISH for *Fer1* and *fru* (close-up view of somata shown in Figure 2). B. (Top) CRISPR knock-in strategy to C-terminally tag

Fer1 with T2A-GAL4. (Bottom) CREa1B cell bodies labelled by the Fer1-GAL4 in green and *fruitless*-expression labeling in magenta with *fru*-lexA. C. Two photon image of neurons labeled by genetic intersection of Fer1-T2A-GAL4 with *fru*-Flp. D. UMAP plot displaying the log-normalized expression of *ara, caup* and *tup* split by time (12 and 48hrAPF). E. UMAP plots displaying the log-normalized expression of *Salm* and *Salr* split by time. F. Lineage labeling using the Awasaki strategy driven by dsf-GAL4 (left), TfAP-2-GAL4 (middle) and tub-GAL4 with the apoptotic block (lexAop-p35) (right). Fer1-T2A-GAL4 and TfAP-2-intersect-dsf-split-GAL4 did not produce lineage labeling. G. Neuronal clusters expressing *fd59a* include CREa1B (arrow). H. UMAP plot displaying the log-normalized expression of *vnd*, showing that *vnd* is not expressed in postmitotic neurons. I. UMAP Featureplots integrated across time showing hemilineage factors in CREa1A.

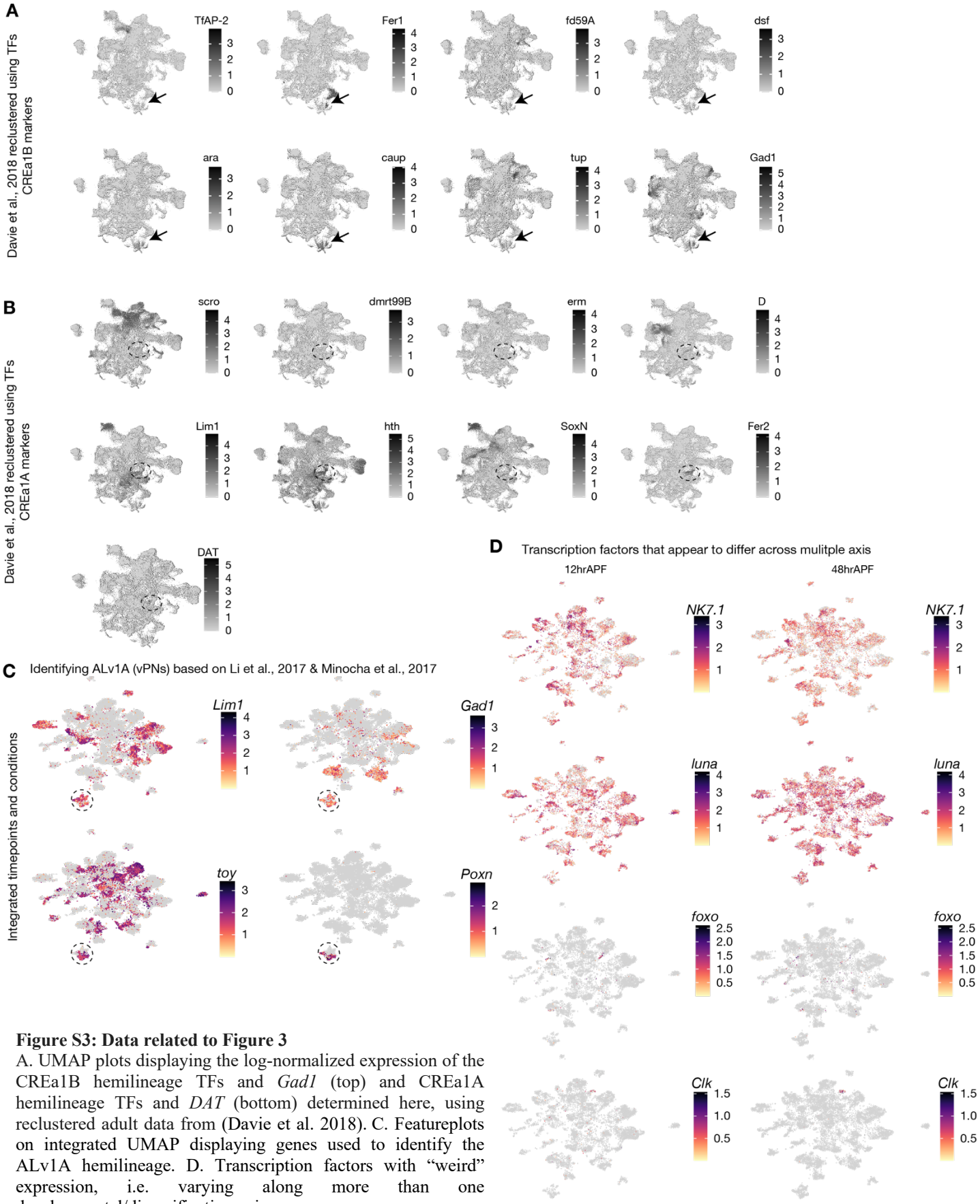

Figure S3: Data related to Figure 3

A. UMAP plots displaying the log-normalized expression of the CREa1B hemilineage TFs and *Gad1* (top) and CREa1A hemilineage TFs and *DAT* (bottom) determined here, using reclustered adult data from (Davie et al. 2018). C. Featureplots on integrated UMAP displaying genes used to identify the ALv1A hemilineage. D. Transcription factors with "weird" expression, i.e. varying along more than one developmental/diversification axis.

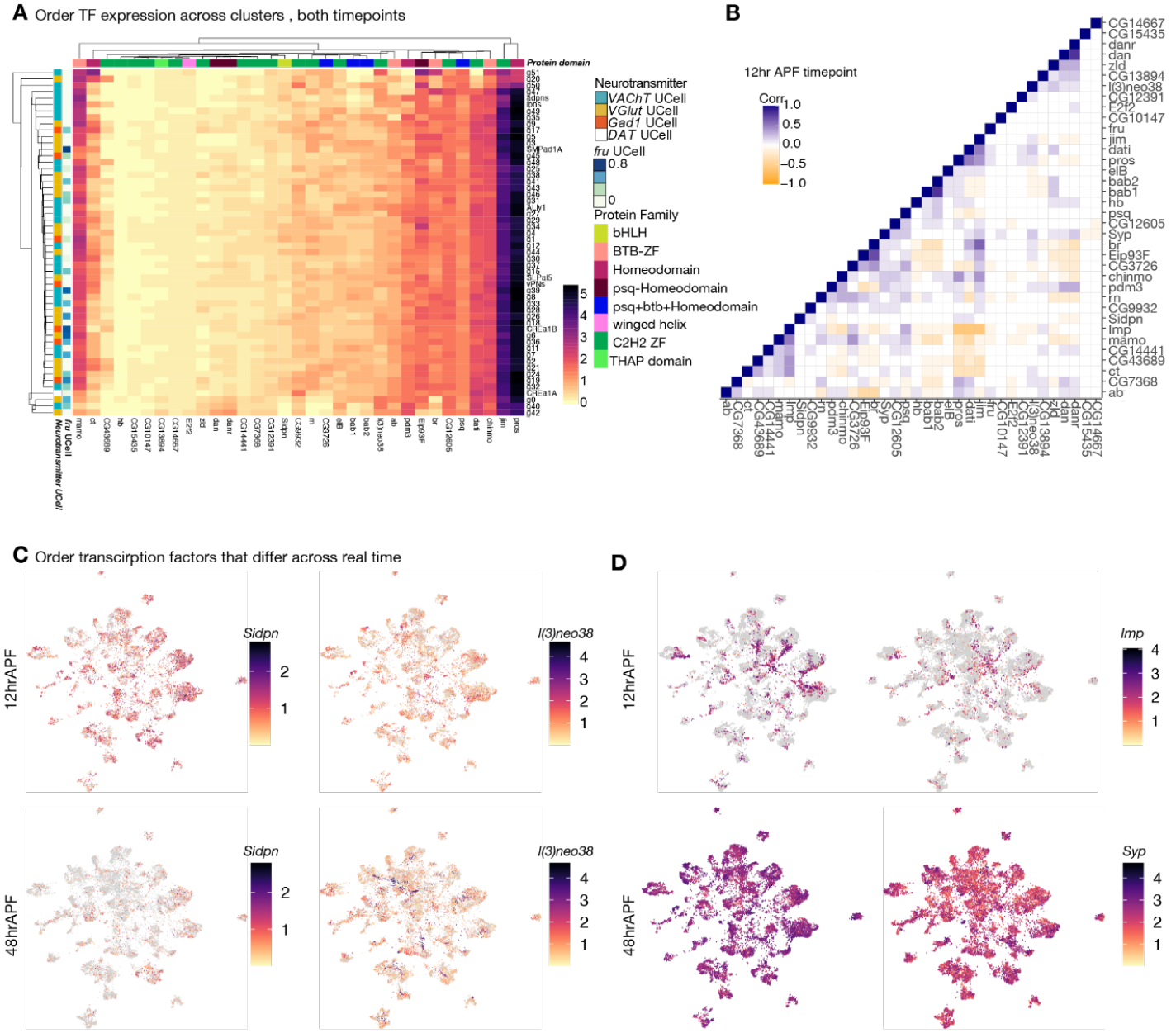

Figure S4: Data related to Figure 4

A. Heatmap displaying expression of birth order factors across integrated clusters (33 TFs, manual curation). Transcription factors were partitioned into protein families using FlyBase labels, displayed below. UCell scores for *fru* and neurotransmitter expression across clusters are shown at left. B. Pairwise correlation analysis between the 33 birth order factors, Imp, Syp and fru. Heatmap shows Pearson's correlation coefficients. C. UMAP plots displaying the log-normalized expression of *Sidpn* and *l(3)neo38* at 12 and 48hrAPF. D. UMAP plots displaying the log-normalized expression of *Imp* and *Syp* at 12 and 48hrAPF.

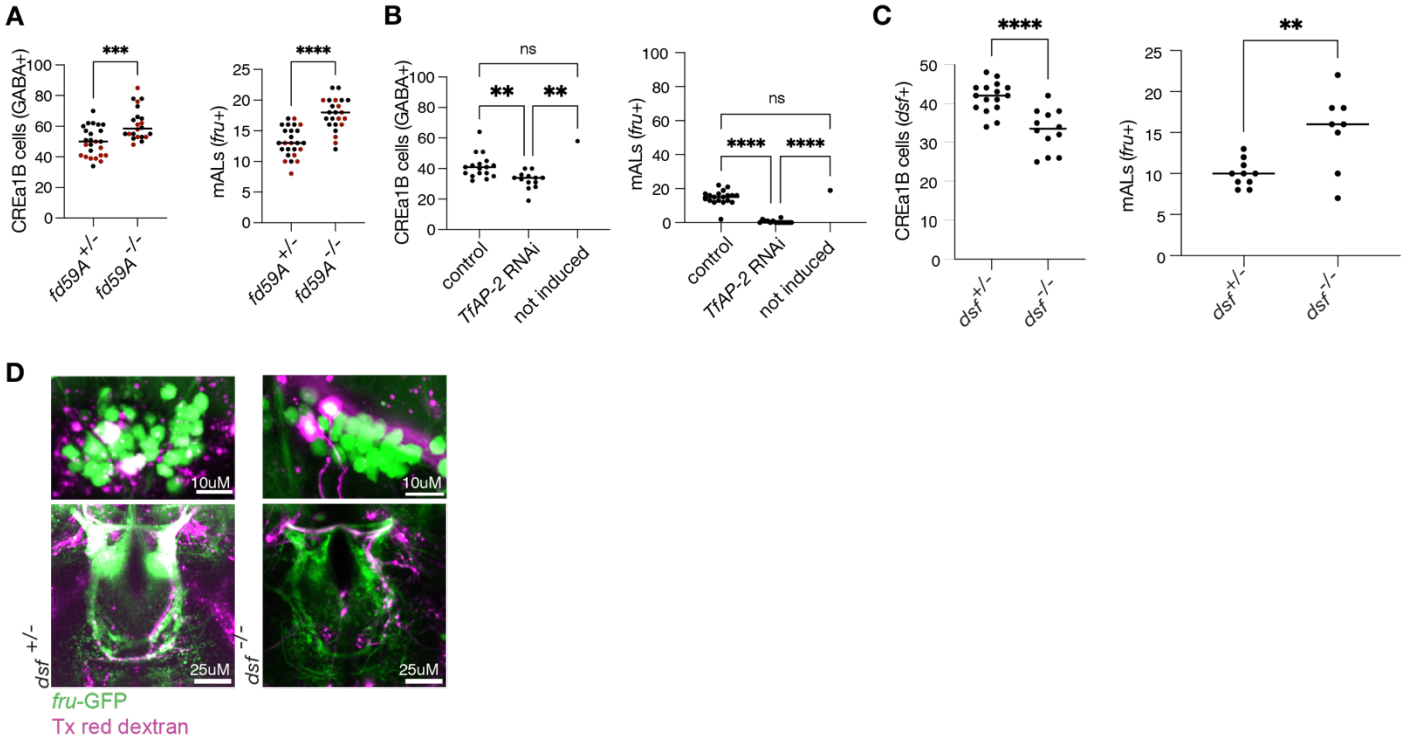

Figure S5: Data related to Figure 5

A. Number of total CREa1B neurons (GABA+) and mALs per hemisphere (*fruitless*-expressing) in *fd59A* control and mutant females. B. The number of total CREa1B neurons (GABA+) and mALs per hemisphere (*fruitless*-expressing) in female *TfAP-2* knockdown clones or controls. C. The number of total CREa1B neurons (*dsf*+) and mALs per hemisphere (*fruitless*-expressing) in *dsf* control or mutant females. D. Zoom in of mAL cell bodies (top) and dendrites (bottom) from males, where Texas red dextran (colored magenta) was electroporated in the mAL axonal tract (*fruitless*-expressing neurons are labelled in green) to allow sparse labelling of mAL neurons in *dsf* het (left) and *dsf* mutants (right).

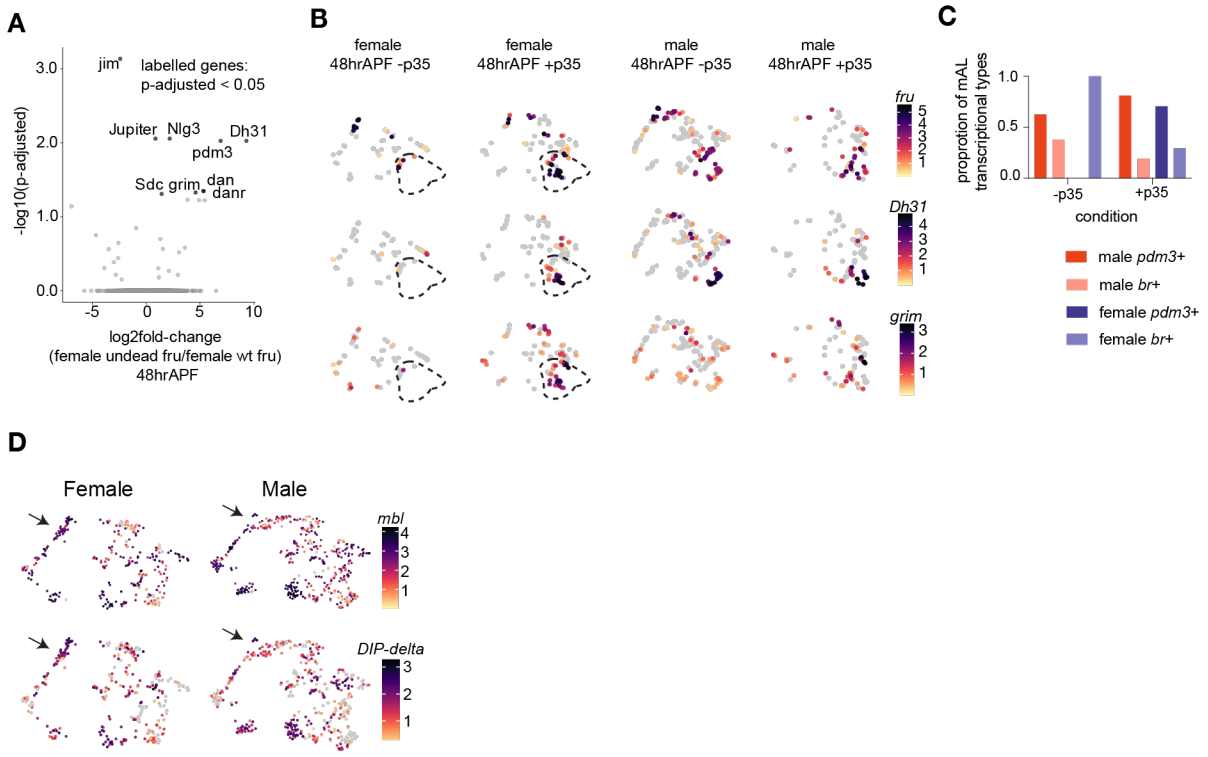

Figure S6: Data related to Figure 6

A. Volcano plot showing differential gene expression between female cells fated to apoptose and female wild type mAL neurons. Labelled genes: p-adjusted < 0.05 based on Wilcoxon Rank Sum test. B. UMAP plots displaying the log-normalized expression of *fru, Dh31* and *grim* in CREa1B across sex (male and female) and condition (+/-p35) at 48hrAPF. C. Proportion of *br+* and *pdm3+* mAL transcriptional subtypes with and without the apoptotic block (p35) in males and females. D. UMAP plots displaying the log-normalized expression of *mbl* and *DIP-delta* split by sex (male and female)

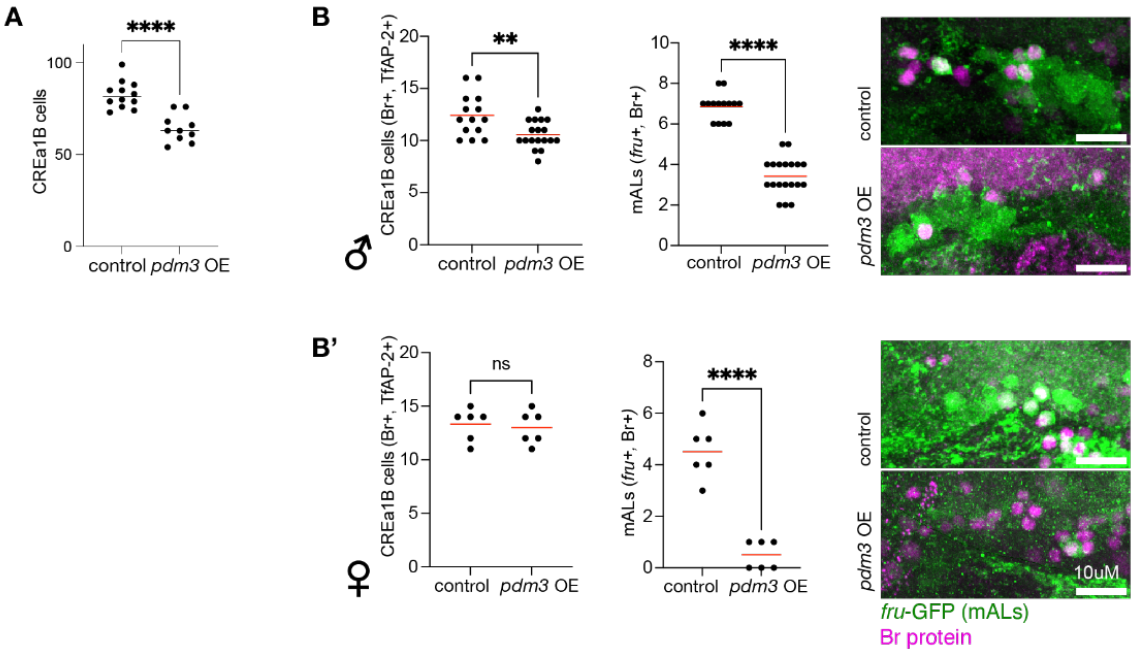

Figure S7: Data related to Figure 7

A. Number of total CREa1B neurons per hemisphere labelled by *dsf* intersect *TfAP-2* split-GAL4 in males in control and *pdm3* overexpression animals. B. Left: Number of Br-expressing CREa1B neurons (based on TfAP-2 protein expression) per hemisphere (left) and number of Br-expressing mAL neurons (*fruitless*-expressing) (right) in males (top) and female (bottom) in control and *pdm3* overexpression animals. Right: mAL cell bodies labeled with the *fru* transcriptional reporter (*fru*-GFP) in green and Br protein in magenta in males (top) and females (bottom) in control and *pdm3* overexpression animals.